



Virginia Commonwealth University
VCU Scholars Compass

Theses and Dissertations


Graduate School

2017

Deletion of Cardiac miR-17-92 Cluster Increases Ischemia/ Reperfusion Injury via PTEN Upregulation

Meeta B. Prakash
Virginia Commonwealth University

Follow this and additional works at: <https://scholarscompass.vcu.edu/etd>

 Part of the [Cardiovascular Diseases Commons](#), [Cell Biology Commons](#), and the [Cellular and Molecular Physiology Commons](#)

© The Author

Downloaded from

<https://scholarscompass.vcu.edu/etd/4956>

This Thesis is brought to you for free and open access by the Graduate School at VCU Scholars Compass. It has been accepted for inclusion in Theses and Dissertations by an authorized administrator of VCU Scholars Compass. For more information, please contact libcompass@vcu.edu.

©Meeta Bharati Prakash 2017

All Rights Reserved

**Deletion of Cardiac miR-17-92 Cluster Increases Ischemia/ Reperfusion Injury via
PTEN Upregulation**

A thesis submitted in partial fulfillment of the requirements for the degree of Master of
Science in Physiology and Biophysics at Virginia Commonwealth University.

by

Meeta Bharati Prakash
B.A. in Biology and Environmental Studies, Dartmouth College, 2013

Director: Anindita, Das, PHD
Assistant Professor
VCU School of Medicine
Division of Cardiology

Virginia Commonwealth University
Richmond, Virginia
June 2017

Acknowledgments

The author wishes to thank several people. Thanks to Dr. Rakesh Kukreja for teaching me in class and sparking my interest in cardiology research. I appreciate his guidance, assurance and acceptance me into his laboratory. Thanks to Dr. Anindita Das, who pushed me and encouraged me, and without whom this thesis would not have happened. She was a constant well of information and assisted me in every aspect of this project, from development to execution. Thanks to Dr. Roland Pittman for serving on my advisory committee and always making physiology jokes at 8am in the morning. Thanks to Dr. Fadi Salloum for creating a wonderful and in-depth course on cardiac function, which changed my focus from dentistry to medicine as a whole. Additionally, I appreciate his expertise in surgery and inspirational work ethic which helped me complete this work. Thanks to Dr. Edward Lefnefsky, Dr. Qun Chen, and Jeremy Thompson for assistance with performing the mitochondrial oxidative phosphorylation study. Thanks to Dr. Arun Samidurai for letting me be his shadow in all experiments and providing his knowledge on protein isolation and performing the molecular studies. Thanks to Sean Roh for lending his surgical expertise and learning alongside me. Thanks to Dr. Jolene Windle and Dr. Mark Subler VCU Transgenic/Knockout Mouse Core for elucidating protocols and data for transgenic mice. Thanks to the Physiology Department, including Christina Kyrus, Dr. Clive Baumgarten, and Harold Greenwald for continuing to advise students and helping them achieve their Master's. Thanks to the entire VCU Pauley Center Cardiology Lab for providing an excellent environment to work and learn. Finally, many thanks to my family for supporting me at every turn of this program and helping me to accomplish all my dreams.

Table of Contents

Abstract	iv
List of Tables and Figures	vi
Introduction	1
1.1 Ischemic Heart Disease	1
1.2 Necrosis and Apoptosis	1
1.3 Mechanisms of Ischemic Injury	5
1.4 Mechanisms of Reperfusion Injury	6
1.5 MicroRNA	9
1.6 Functions of the miR-17-92 Cluster	9
1.7 Phosphatase and tensin homolog (PTEN) Pathway	12
Materials and Methods	15
2.1 Animals	15
2.2 Genotyping Selective Knockout Mice and Experimental Groups	15
2.3 Tamoxifen	17
Experimental Design:	17
2.4 Ischemia and Reperfusion via simulated Myocardial Infarction	20
2.5 Infarct Size Measurement	20
2.6 Echocardiography	21
2.7 RNA Isolation	21
2.8 Mitochondrial Isolation and Oxidative Phosphorylation Measurements	24
2.9 Cardiomyocyte Isolation	25
2.10 Cardiomyocyte Simulated Ischemia and Reoxygenation	26
2.11 TB staining	26
2.12 TUNEL staining	26
2.13 JC-1 staining	27
2.14 Protein Isolation and Western Blots	27
2.15 Data Analysis and Statistics	29
Results	30
Discussion	51
References	56

Abstract

DELETION OF CARDIAC miR-17-92 CLUSTER INCREASES ISCHEMIC/REPERFUSION INJURY VIA PTEN UPREGULATION

By: Meeta Prakash, M.S.

A thesis (or dissertation) submitted in partial fulfillment of the requirements for the degree of (list degree, for example, Master of Science, Doctor of Philosophy, Master of Social Work) at Virginia Commonwealth University.

Virginia Commonwealth University, 2017

Major Director: Anindita Das, PhD
Assistant Professor
VCU School of Medicine
Division of Cardiology

The miR-17- 92 cluster is necessary for cell proliferation and development of the cardiovascular system. Deletion of this cluster leads to death in neonatal mice. The role of this cluster still needs to be defined following ischemia and reperfusion. **Methods and Results:** Adult male mice were injected with Tamoxifen- was to induce inducible cardiac-specific miR-17- 92-deficient (miR-17- 92-def: MCM:TG:miR-17- 92 flox/flox) and wild type (WT: MCM:NTG:miR-17-92 flox/flox) mice were subjected to 30 minutes of myocardial ischemia via left anterior descending coronary artery ligation followed by reperfusion for 24 hours. Post I/R survival (48%) and ejection fraction were reduced, while myocardial infarct size enlarged in miR-17- 92-deficient mice as compared to WT mice (survival: 71%). Necrosis (trypan blue

staining) and apoptosis (TUNEL assay) both were higher in adult cardiomyocytes isolated from miR-17-92-deficient mice as compared to WT mice subjected to simulated ischemia/reoxygenation with a concomitant reduction of mitochondrial membrane potential (JC1 staining). The electron transport chain was compromised through dysregulation of glutamate+malate as complex I substrate and malate dehydrogenase in the hearts of miR-17-92-deficient mice compared to WT. After 4 hours of reperfusion, PTEN expression, a downstream target of miR-20A, increased, while phosphorylation of AKT reduced in the hearts of miR-17-92-deficient mice in comparison to WT. The induced knockdown of cardiac miR-17-92 increases myocardial I/R injury by ceasing suppression of PTEN, leading to decreased concentrations of AKT and mitochondrial dysfunction. These results suggest that innovative therapeutic strategies can focus on genetic upregulation of miR-17-92 in patients with coronary artery disease.

List of Tables and Figures

Figure 1: The Extrinsic and Intrinsic Pathways of Apoptosis

Figure 2: Cardiac Ischemia Cycle

Figure 3: PTEN Pathway and Targets

Figure 4: Experimental Design with Timepoints

Figure 5: Genomic Map of Cluster miR-17-92

Table 1: Primary and Secondary Antibodies for Western Blot Analysis

Figure 6: Representative figure of agarose gel with PCR products using CRE primers

Figure 7: Representative Figure of Agarose Gel for Mutant miR-17-92 Cluster

Figure 8: Representative Agarose Gel for Transgenic Genotyping

Figure 9: MicroRNAs in Hearts of WT and miR-17-92-def mice

Figure 10: Mitochondrial Oxidative Phosphorylation

Table 2: Survival Rates of Mice

Figure 11: Infarct Size and Risk Area Measurement following I/R Injury

Figure 12: Cardiac Function of WT and miR-17-92-deficient Mice before I/R and after I/R Injury

Figure 13: Cardiac Function of WT and miR-17-92 Mice before and after I/R

Figure 14: Echocardiography Measurement of Left Ventricle before and after I/R

Figure 15: Assessment of Cardiomyocyte Necrosis by trypan blue (TB) Staining

Figure 16: Assessment of Cardiomyocyte Apoptosis using TUNEL Staining

Figure 17: Assessment of Mitochondrial Membrane Potential using JC1 Staining

Figure 18: The Expression of miR-17-92 Downstream Targets PTEN and AKT

Figure 19: The Expression of MDH, GDH and PDH in Cardiac Mitochondria of WT and miR-17-92-def Mice

Introduction

1.1 Ischemic Heart Disease

According to the Center for Disease Control, heart related diseases are the leading cause of death in the United States at just over 600,000 deaths in 2014 alone¹. Worldwide, ischemic heart disease killed almost 9 million people in 2015². Many heart diseases involve pressure or volume overload causing hypertrophy of the heart, leading to heart failure³. Coronary Artery Disease (CAD) contributes to myocardial infarction (MI) and ischemia through occlusion of blood vessels that provide oxygen to cardiac muscle cells. This reduction of blood flow usually stems from thrombosis in an artery in conjunction with an atherosclerotic plaque⁴. The current treatment for myocardial infarction is restoration of blood flow. The process of reperfusion, however, can be harmful and cause cells to undergo apoptosis. Even if a person survives an infarction, the resulting damage to the myocytes and extracellular matrix can lead to progressive ventricular dilation and eventual heart failure⁵. The degradation and heart failure can significantly reduce quality of life and even cause death. These patients rely on medical intervention to sustain life. Therefore the public health system remains concerned about not only preventing myocardial infarctions, but also limiting the aftermath of this event. Cardioprotective therapies and post-ischemic conditioning have become large focuses of the scientific community, and discovering novel ways to better understand myocardial infarction remains paramount.

1.2 Necrosis and Apoptosis

The cell cycle regulates the stages at which the cell will grow, replicate DNA and divide into daughter cells. However, sometimes this process can be halted by death of the cell. This usually occurs by either necrosis or apoptosis. Myocardial injury stems from an increase in both necrosis and apoptosis. Upon reperfusion, the immediate lethal myocardial injury is necrotic, while

delayed injury is apoptotic⁶. Focusing on delayed injury allows therapies to be used in conjunction to prevent further damage to the heart⁶. Hallmarks of necrosis include cellular swelling until the cell lyses, ATP depletion, random DNA fragmentation, and areas of tissue are affected. Necrosis can attract neutrophils and lead to inflammation. In apoptosis, cellular condensation means that the membranes remain intact as it is systemically phagocytosed with ladder-like DNA fragmentation. Apoptosis is a gene directed process and sometimes individual organelles are still functional. Typically a stimulus will begin the intracellular response through signal transduction and activate transcription factors. Apoptosis can play a positive role by helping with tissue remodeling and eliminating cells that are damaged or no longer required.

Several signaling pathways can cause the cells to undergo apoptosis. There can be a withdrawal of signals like growth factors or interleukin-2 or receipt of negative signals like increased oxidant levels, DNA damage, or death activators, and lymphotoxin like TNF- β . The extrinsic pathway consists of death ligands attaching to receptors and initiating a caspase 8 mediated pathway through the caspase 3 to programmed cell death. The extrinsic pathway bound caspases become activated through an “induced proximity” mechanism by aggregation⁷. Common ligands include Fas, tumor necrosis factor alpha (TNF- α), and TNF related apoptosis inducing ligand (TRAIL)⁸.

The intrinsic pathway begins with DNA damage and p53 activation, which causes mitochondrial depolarization and release of cytochrome C or Smac/DIABLO into the cytoplasm. Cytochrome C can also be released through a disruption in the pro-apoptotic protein Bax and anti-apoptotic protein Bcl-2 ratio⁹. Sometimes, ATP depletion can initiate the the movement of Bax from the outer mitochondrial membrane and cause cytochrome c to be released¹⁰. If the release channels are not formed through Bax/ Bcl2 heterodimerization, cytochrome c can be released

through outer membrane rupture due to opening of the mitochondrial permeability transition pore⁹. Cytochrome c binds to adaptor protein (Apaf-1), aggregates with procaspase 9, and activates caspase 9 and caspase 3 programmed cell death¹¹. Smac/DIABLO inhibits inactivators of apoptosis (IAPs) which prevents cleavage of procaspase 3⁸. Caspase 3 finishes the cascade by inducing apoptosis through cleavage of PARP, an enzyme that is also activated by DNA damage¹⁰. In type 1 cells, death receptor ligation is enough to lead to cell death, but in type 2 cells death is dependent on the mitochondrial pathway through Bax and Bcl-2. If caspase 8 activation occurs in type 2 cells, caspase 8 interacts with Bid, an agonist of Bax⁸. After damage occurs in the heart, too much apoptosis can lead to wall thinning and cardiac remodeling, which can lead to heart failure. However, dysregulation in apoptosis can also lead to hyperplasia and cancer¹⁰. Caspase inhibitors have been reported to attenuate myocardial ischemia/reperfusion injury, however, once the apoptotic cascade has been initiated it is irreversible¹⁰. Reperfusion has been shown to accelerate the apoptotic process and thus focusing on ischemia and reperfusion injury is important to prevent further heart failure¹⁰.

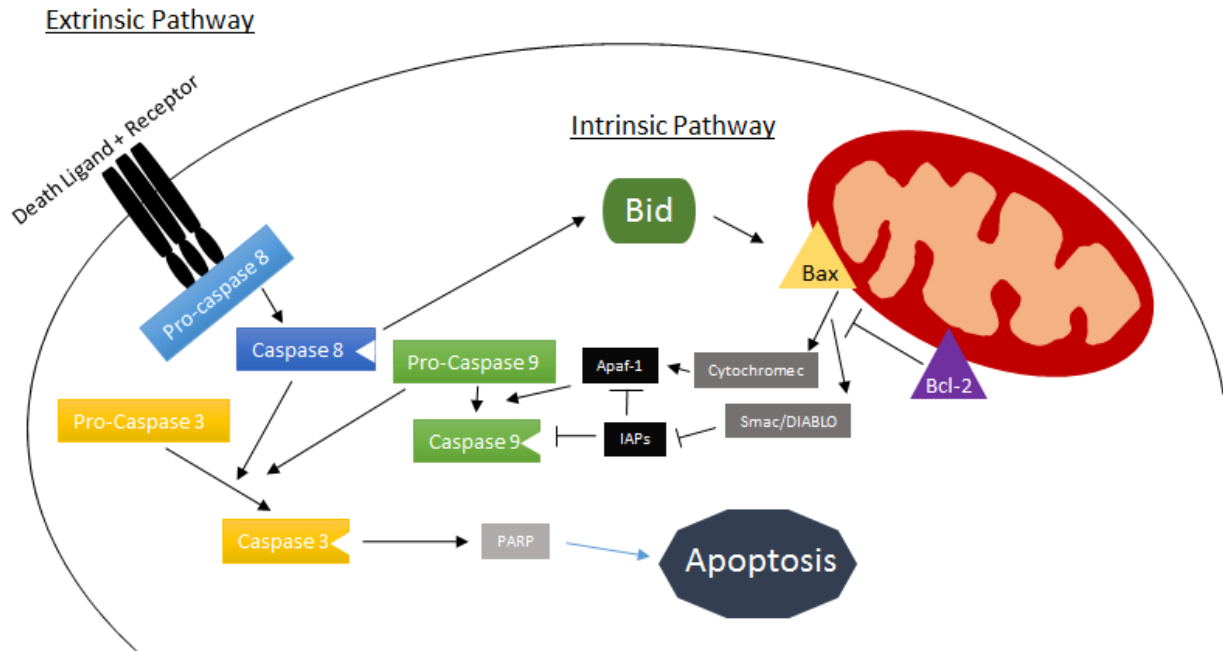


Figure 1: The Extrinsic and Intrinsic Pathways of Apoptosis Programmed cell death can be executed via outside signals or via cell corruption indicating that damage to organelles or DNA are too extensive. Both ultimately end in a caspase 3 mechanisms with PARP cleavage.

1.3 Mechanisms of Ischemic Injury

The four described categories of myocardial ischemic and reperfusion injury include 1) reperfusion arrhythmias, 2) myocardial stunning due to contractile dysfunction, 3) microvascular obstruction leading to ischemia and 4) lethal reperfusion injury causing apoptosis even after ischemia ends. Among these, microvascular obstruction and reperfusion injury are potential targets for significant therapeutic interventions as the primary determinant for the size of the infarct are the length of ischemia and attenuation of reperfusion injury. In ischemia, lack of blood from the occluded arteries causes myocytes in that area to be at risk of a heart attack⁴. Due to the high demand of myocyte contractile activity, ATP must be continuously supplied by mitochondria, which are distributed in high concentrations throughout in either the sarcolemma or in between fibers. If prolonged ischemia occurs from microvascular obstruction, myocyte death starts in the endocardium and continues to the epicardium as oxygen supply remains low. This begins when oxidative phosphorylation stops, ending generation of ATP and destabilizing the mitochondrial membrane.

The electron transport chain, consisting of four protein complexes that help produce ATP, becomes vulnerable and damaged during the period of ischemia¹². Complex I oxidizes NADH, passing the electron to coenzyme Q which reduces complex III, then cytochrome c and finally becomes oxidized by complex IV to produce water. Complex II also reduces coenzyme Q. The sum of all these reactions creates a proton gradient due to the transfer of hydrogen ions from the matrix of the inner membrane. Cellular metabolism starts utilizing anaerobic glycolysis, and the buildup of lactate in the cytosol causes the pH to drop¹². The high concentration of hydrogen ions utilizes the membrane-bound Na^+ and H^+ antiporter, which exchanges the ions and causes sodium to increase. Because ATP is in limited quantity, the sodium calcium antiporter tries to dispose of

the excess sodium and results in a large buildup of calcium, which closes the Mitochondrial Permeability Transition Pore (MPTP). The MPTP normally remains closed, and helps to ensure the selectivity and ionic gradient. Physiological gradients are disrupted and myocyte contractions end. This disruption of metabolic processes and reduction of ATP then can act as the impetus for a biochemical chain that leads to programmed cell death. Though activation of apoptosis begins during ischemia, 25-40% of eventual cardiac death stems from reperfusion⁴.

1.4 Mechanisms of Reperfusion Injury

In patients experiencing microvascular obstruction, timely reoxygenation, or reperfusion, to the myocardium helps mitigate infarct size and heart failure¹³. Reperfusion is necessary in order for the heart to survive, however, it can also further increase infarct size. To understand the negative effects of reperfusion, the progression of programmed cell death, or apoptosis, must first be explored. During restoration of blood flow, the electron transport chain, located on the inner mitochondrial membrane restarts and generates excessive reactive oxygen species¹². As blood enters and washes out the lactic acid, the pH returns to neutral and causes the reactive oxygen species to increase calcium concentrations, which leads to the MPTP opening and inner mitochondrial membrane depolarization. The decreased permeability of the mitochondria also causes the organelle to swell, destabilizing the outer mitochondrial membrane.

Though ischemia initiates apoptosis, reperfusion further aggravates the process by changing the normal ratio of mitochondrial apoptotic proteins such as Bax and Bcl2 leading to the caspase-3 or caspase-8 enzyme execution of cell death¹⁴. The swelled mitochondria eventually bursts, releasing pro-apoptotic proteins like cytochrome c and Bax¹³. The potential for therapies that target the Bax and Bcl2 ratio, prevent the opening of the MPTP, and attenuation of the reactive oxygen species remains high⁴.

Mitochondria play an important role in the energetics of a cell by producing 95% of ATP, though these organelles also consume 90% of the oxygen¹⁵. Two potential sites of free radical oxygen generation are in the electron transport chain in the mitochondria. During ischemia, the mitochondria try to produce ATP, but without a steady supply of oxygen, NADH dehydrogenase in complex I and cytochrome *b-c₁* in complex III will produce free radicals¹⁶. These reactive oxygen species injure the cell by reducing mitochondrial membrane potential and causing the release of cytochrome c into the cytosol, leading to apoptosis. In the myocyte, there are also antioxidant enzymes such as superoxide dismutase and glutathione peroxidase that protect the cell from damage by reducing hydrogen peroxide and free radicals¹⁷. Current ideas for treatment include giving antioxidants at the time of myocardial reperfusion to prevent the apoptotic cascade, treating with solutions stopping the actions of the electron transport chain, and preconditioning cells to ischemia to reduce abundance of reactive oxygen species. However, methods like these are either proving to have mixed results clinically or remain difficult as it is hard to predict complete microvascular obstruction¹². Unfortunately, options to reduce the infarct size are limited and thus techniques to boost cardioprotection in ischemia and reperfusion are still important to investigate.

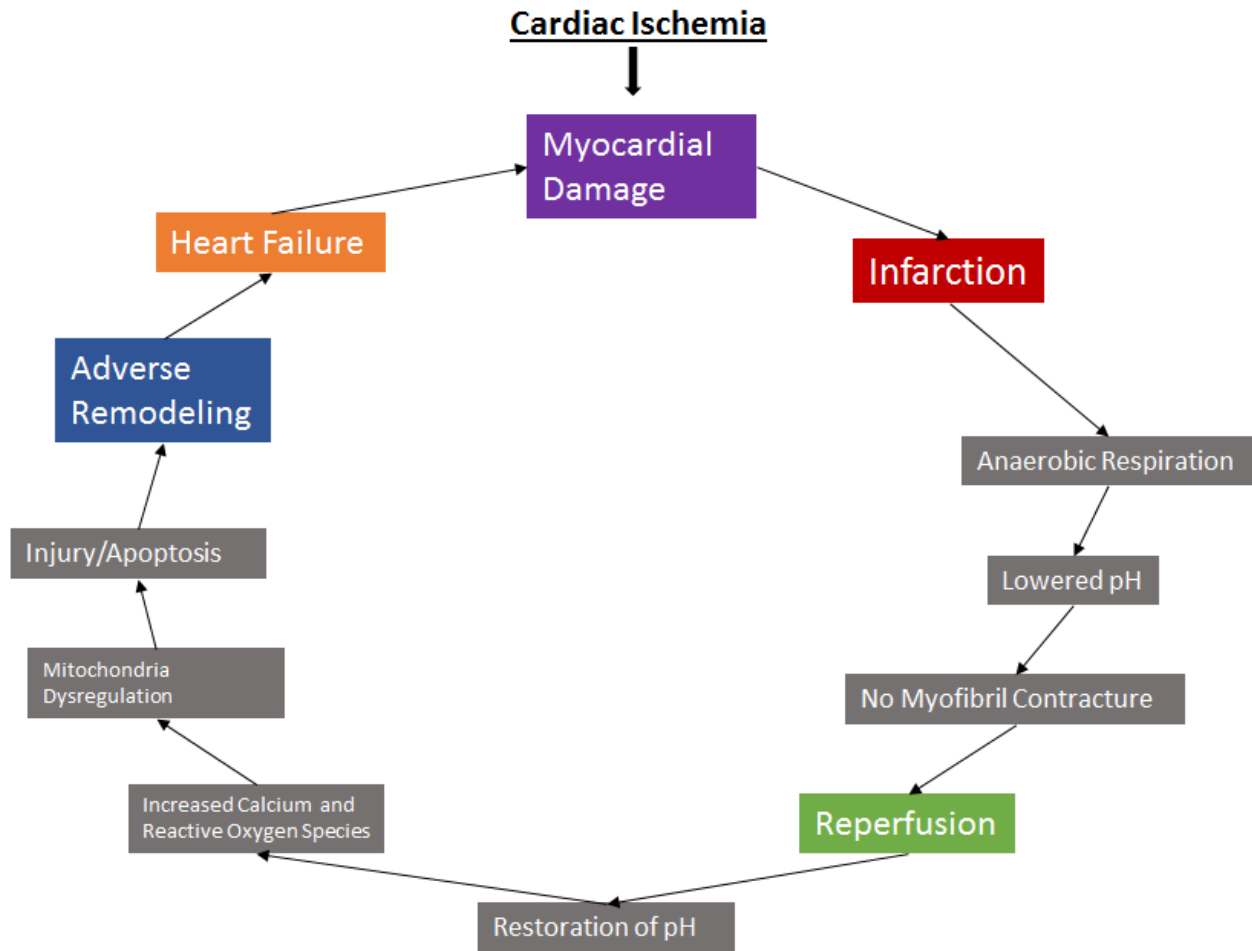


Figure 2: Cardiac Ischemia Cycle Once heart damage begins, a positive feedback cycle can occur where myocardial damage leads to additional heart failure. The infarct region from ischemia does not contract and the heart attempts to compensate through adverse remodeling, such as hypertrophy that can lead to more opportunities for myocyte damage.

1.5 MicroRNA

MicroRNA (miR) are small non-coding RNAs about 20-24 nucleotides long that controls gene expression. Often, their role is to regulate post-transcriptional gene expression through binding the 3' UTR of mRNA causing their inhibition or degradation. Thousands of microRNAs have been discovered, though not all their functions and targets have been elucidated. The miRs are synthesized via transcription of the pri-micro-RNA in the nucleus as a hairpin structure, gets cut by Drosha, and exits the cell via Exportin- 5 as pre-miRNAs. Once in the cytoplasm, Dicer cleaves the pre-miRNAs into smaller double stranded RNA called RNA duplexes. These structures then can be used by the RNA- induced silencing complex (RISC) to bind to the mRNA¹⁸. Sometimes the sequences can be perfectly complementary at the binding region leading to degradation of mRNA, or can bind imperfectly at the nucleotide positions 2-7 in the seed region resulting in the suppression of the gene expression¹⁹. miRNA with similar nucleotides at this location are said to have the same seed sequence, may have similar targets and are categorized to the same family.

Many microRNA, such as miR-1, miR-208, miR-133a and miR- 27b, have already been identified as having an instrumental roles in cardiac development and function^{20,21-23}. Some of these roles include cell proliferation, conduction, and differentiation.

1.6 Functions of the miR-17-92 Cluster

The miR- 17-92 family, also known as oncomir-1, is located on chromosome 13 and comprised of six microRNAs, including miR-17, miR- 18a, miR- 92a, miR- 106, miR- 19a/b, and miR-20a/b²⁴. This cluster originally was discovered as a human oncogene causing cells to bypass the apoptotic checkpoint, but later it was found necessary to form cardiomyocytes in embryonic mice²⁵. Additionally, this cluster is required for further proliferation of cardiomyocytes

during the postnatal stage, and as a critical part of bone morphogenetic protein (BMP) signaling²⁶. This cluster also seems to be partially responsible for angiogenesis through endothelial cells, matrix remodeling, and hematopoiesis^{27,28}. Mutant miR-17-92 postnatal mice hearts were shown to be reduced in size compared to their controls²⁹. This cluster can be regulated by vascular growth endothelial factor-A (VEGF), Elk-1 mitogen stimulation, fibroblast growth factor 2, and extracellular signal regulated kinase^{19,30}. The E2F family of transcription factors regulate cell cycle progression and apoptosis, and interacts closely with miR-17-92^{31,32}. Downregulation of this cluster can cause upstream regulators like VEGF to induce angiogenic responses in endothelial cells and change developmental responses³⁰. Deletion of this cluster leads to apoptosis in Myc-driven lymphoma cells, as miR-17-92 accelerates Myc-induced B cell lymphomagenesis^{33,34}. PTEN, a tumor repressor, was also identified as a potential target for the cluster, and specifically miR-19a/b²⁹.

Three subdivisions of the miR-17-92 clusters, miR-17, miR-19, and miR-93 were shown to suppress apoptosis^{22,23,24,26}. The members of the miR-17 found to inhibit tumor cell death through enhancing the Stat3 and resisting the MEK pathway³⁵. Additionally, it was found to inhibit a pro-apoptotic protein Bim and dysregulate the p53 pathway which leads to cell cycle arrest³⁶. Bim protein levels were increased in embryos that had targeted deletions of the miR-17-92 cluster^{37,38}. Bim acts by antagonizing antiapoptotic proteins like Bcl-2. MiR-17 was found to be significantly upregulated after myocardial infarctions, and decreases tissue inhibitor of metalloproteinases to increase cardiac remodeling⁵. MiR-17 concentration was significantly lower in the plasma of patients with coronary artery disease, suggesting a role in atherosclerosis³⁹. Approaches to reduce miR-17 after a myocardial infarction may help prevent subsequent heart failure due to ventricular dilation. MiR-20a specifically was found to regulate Fas expression

creating the malignant cell type in osteosarcoma cells and piquing interest in the potential capability to pause apoptosis in cardiomyocytes^{36,40}. MiR-20a also inhibits hypoxia-induced apoptosis through targeting Egl3/PHD3, a prolyl hydroxylase domain protein³⁹. Three PHDs (PHD1, PHD2, and PHD3) catalyze the degradation of HIF by hydroxylating proline residues in the HIF-1 α subunit in the normoxic state. In hypoxia, PHDs cannot perform and HIF-1 α accumulates and increases target gene expression. PHD3 concentration is linked with apoptosis as it is found to be upregulated in cardiomyopathy, myocardial I/R injury and congestive heart failure⁴¹. PHD3 interacts with Bcl-2 and prevents formation of the anti-apoptotic complex Bax-Bcl-2⁴¹. PHD2 inhibition has been shown to mitigate I/R injury, so regulation of PHD3 through miR-17-92 could be a potential therapeutic target⁴². The overexpression through adenoviruses of miR-17 and miR-20a both also downregulated E2F1³¹. E2F1 overexpression can play a role in increasing apoptosis. The mir-19 family also works through the Stat3 and Bim proteins. MiR-18 and miR-19 downregulate the anti-angiogenic factors thrombospondin-1 (Tsp-1) and connective tissue growth factor (CTGF), causing increased blood vessel growth and tumor angiogenesis⁴³. The mir-19 and mir-92 families both inhibit TNF related proteins to reduce incidence of programmed cell death⁴⁴. Oligonucleotides can antagonize miR-92a to promote blood vessel growth and recovery from ischemia⁴⁵. The proven capability of the miR-17-92 families to reduce apoptosis suggests that this cluster might help reduce cardiomyocyte death in the case of ischemia. Reduced myocardial infarction by coronary artery occlusion and preserved post-MI cardiac function results from miR-17-92 overexpression²⁹. However, the role of this cluster is still uncertain because of the differential expression of cluster targets on angiogenesis needs to be investigated further.

Although miRNAs can be found throughout the body, cluster expression can vary greatly by tissue type. Furthermore, sample concentrations of the miR-17-92 cluster in canine tissue show

that miR-20 is the most highly expressed of the cluster in the heart¹⁸. Murine samples also show miR-20 to be densely concentrated in the lung and heart, demonstrating potential for miR-20 be used in cardioprotection⁴⁶. Disentangling the roles of the miR-17-92 cluster can have a significant impact on the way that physicians could treat patients following an infarction, like therapeutic inhibition of specific microRNA clusters.

1.7 Phosphatase and tensin homolog (PTEN) Pathway

MiR-17-92 regulates heart size by repressing PTEN and cardiac impulse propagation through interacting with Connexin-43 (Cx43)³⁷. PTEN is a tumor suppressor and inhibitor of the Phosphoinositide-3- Kinase (PI3K)/ Akt/ mTOR pathway and is necessary for regulation of cardiomyocyte size and contractility³. PTEN knockout has been identified in human cancers, leading to increased downstream signaling and the metastatic phenotype⁴⁷. PTEN prevents myocyte proliferation, vascular growth, and angiogenesis by obstructing PI3K/AKT^{48,49}. In cardiomyocytes, PI3K γ is a lipid kinase that functions in cellular signaling like proliferation, cell size and prevention of apoptosis³. Phosphorylated lipids are found in the cellular membrane and recruit other components to further the stimulus during the signaling event⁴⁷. PTEN acts as a phosphatase to decrease the concentration of lipids and stops the PI3K pathway, and in knockout mice is lethal. A downstream target of PI3K γ is cAMP, which when inhibited, led to the decreased contractility and when enhanced activated PKA and phospholamban to intensified contractility^{3,50}. The AKT pathway is a target of the PI3K signaling molecule which can influence many downstream proteins, and when activated creates higher concentrations of phosphorylated AKT. AKT activation improves cardiac function, infarct size, and decreases apoptosis following an ischemia and reperfusion event⁵¹⁻⁵³. When AKT phosphorylates Bad, it inhibits the BAD/ Bcl-2 complex and allows the Bcl-2 protein to participate in a cell survival response⁴⁷. PTEN repression

causes increased levels of phosphorylated AKT, which elevates myocardial microvascular density and mitigates remodeling following myocardial infarction⁵⁴. Thus, the loss of miR-17-92 could influence the PTEN pathway and lead to changes in fractional shortening and cardiac size. Looking closely at the effects of miR-17-92 and PTEN in apoptosis could help to attenuate myocardial infarction injury.

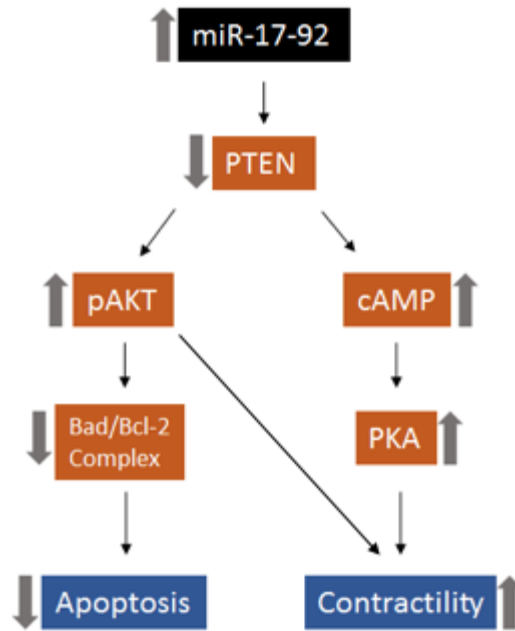


Figure 3: PTEN Pathway and Targets Following overexpression of the miR-17-92 cluster in myocardial ischemia and reperfusion injury, downstream changes lead to increased cardiac function and contractility and decreased apoptosis.

Materials and Methods

2.1 Animals

Adult male *mir-17~92^{fl/fl}* mice flanked by *loxP* sites crossbred with α MHC-MerCreMer cre recombinase tamoxifen inducible mice were received from Augusta University (formerly Georgia Regents University in Augusta, Georgia, stock numbers 008458 and 005650). The C57BL/6J mice were supplied by The Jackson Laboratory (Bar Harbor, ME). The animal care and experiment protocols were approved by the Institutional Care and Use Committee of Virginia Commonwealth University.

2.2 Genotyping Selective Knockout Mice and Experimental Groups

A portion of the tail was used to isolate DNA to correctly segregate mice into *miR-17~92^{fl/fl}* groups (double transgenic), detect the presence of the cre recombinase gene, and confirm the knockdown of the *miR-17-92* cluster. First 75 μ l of a solution of 25mM NaOH and 0.2mM EDTA (pH of 12) was added to the tail segment and then incubated at 95°C for 30 minutes. After cooling this solution on ice, 75 μ l of a second neutralizing solution of 40mM Tris-HCl (pH of 5) was added and then vortexed. The solution was then centrifuged for 5 minutes at 12,000g. 2 μ l of this sample was then added into the PCR mix specific to the number of reactions and type of reaction. The enzyme mix includes nuclease free water, dNTPs, Dream Taq DNA Polymerase, and 10X buffer to create a final volume of 25 μ l. The polymerase chain reaction would be run according to the appropriate Jackson Laboratory genotyping protocol for the specific mice^{55,56}.

For *miR-17-92^{fl/fl}*, three primers were utilized; oIMR8528 (sequence: TCGAGTATCTGACAATGTGG), oIMR8529 (sequence: TAGCCAGAAGTTCCAAATTGG), and oIMR8530 (sequence: ATAGCCTGAAACCAACTGTGC). Initial denaturation occurred for 3 minutes at 94°C, and was followed by 40 cycles of 94°C denaturation for 30 seconds, 56°C

annealing for 1 minute, and 3 minutes of extension at 72°C. The final extension took place for 5 minutes at 72°C and kept at 4°C until electrophoresis. The mutant gene would appear at 289 base pairs, while the wild type would be at 255 base pairs after PCR and electrophoresis. This method was utilized to eliminate any mice that did not have the mutant strain of the miR-17-92 cluster that was flanked by loxP sites. LoxP sites allow for a conditional deletion through the cre recombinase technology. Through the administration of tamoxifen, the CRE transgene will influence the cardiac-specific alpha myosin heavy chain promoter and knocks down the expression of the loxP flanked site, the miR-17-92 cluster.

To confirm the tamoxifen-inducible CRE recombinase gene, two primers were used; CRE (608-630 sequence: ATATCTCACGTA CTGACTGACGGTGGG) and CRE (1054-1032 sequence: CTGTTTCACTATCCAGGTTACGG). Initial denaturation occurred for 2 minutes at 94°C, which was followed by 35 cycles of 94°C denaturation for 1 minute, 60°C annealing for 1 minute, and 2 minutes of extension at 72°C. The final extension took place for 7 minutes at 72°C and kept at 4°C until electrophoresis. After running through the gel, the CRE mutant would appear at 448 base pairs.

Finally to confirm CRE recombinase in the correct location (MYH6-CRE), four primers were used CRE (608-630), CRE (1054-1032), A1CF (4879-4902) and A1CF (5108-5085). Initial denaturation occurred at 95°C for 3 minutes, and was followed by 40 cycles of 95°C denaturation for 30 seconds, 60°C annealing for 30 seconds, and 1.5 minutes of extension at 72°C. The final extension took place for 5 minutes at 72°C and kept at 4°C until electrophoresis. The CRE transgene would be at 448 base pairs, while the non transgenic band would appear at 230 base pairs. Samples could be hemizygous, homozygous, or nontransgenic. To confirm the deletion of miR-17-92 cluster in the heart with MYH6-CRE following tamoxifen treatment, DNA was extracted from

cardiac tissue samples using the Qiagen DNeasy Blood & Tissue kit (Catalog number 69504) and the miR-17-92^{flox}.

The CRE recombinase samples were then run through a 1.5% agarose gel on a Bio-Rad electrolysis machine with TBE running buffer for 30 minutes at 100 volts. The miR-17-92^{flox} and MYH6-CRE samples were then placed in a 1.75% agarose gel and underwent electrolysis for 50 minutes at 100 volts with TBE running buffer. The amplified cDNA sizes were then visualized in the gel using Spectroline[®] UV transilluminator.

The mice were separated into two groups; the first contained both the mutant miR-17-92 cluster and the appropriate transgene for CRE recombinase technology, and the second were the mice that did not test positive for the appropriate CRE recombinase gene. The first group was then put through a tamoxifen regimen to reduce concentrations of the miR-17-92 cluster. The two separate groups are demarcated as miR-17-92-deficient (miR-17-92-def: MCM:TG:miR-17-92 flox/flox) mice and wild type (WT: MCM:NTG:miR-17-92flox/flox) mice.

2.3 Tamoxifen

Adult male mice were injected with 20 mg/kg concentration of tamoxifen via intraperitoneal injection for five consecutive days to create miR-17-92 deficient mice. The tamoxifen T5648 was purchased from Sigma- Aldrich[™].

Experimental Design:

For *in vivo* study, adult male WT and miR-17-92-def mice (body weight~ 35 g, ~ 8-10 months old, after 1-week of tamoxifen treatment (20 mg/kg, i.p. for 5 days)) were subjected to *in vivo* ischemia for 30 minutes and reperfusion for 1 hour to examine protein expression and phosphorylation or reperfusion for 24 hours for measurement of cardiac function and infarct size. For *in vitro*

methodology, mitochondria were isolated from tamoxifen-treated adult WT and miR-17-92-def mice and oxidative phosphorylation and mitochondrial proteins were analyzed.

Primary cardiomyocytes were isolated from tamoxifen-treated WT and miR-17-92-def mice and after 40 min simulated ischemia (SI) and 1 hr reoxygenation (RO), necrosis and mitochondrial membrane permeability were assessed by trypan blue staining and JC-1 staining, respectively.

Cardiomyocyte apoptosis were assessed by TUNEL assay following 18 hours of RO.

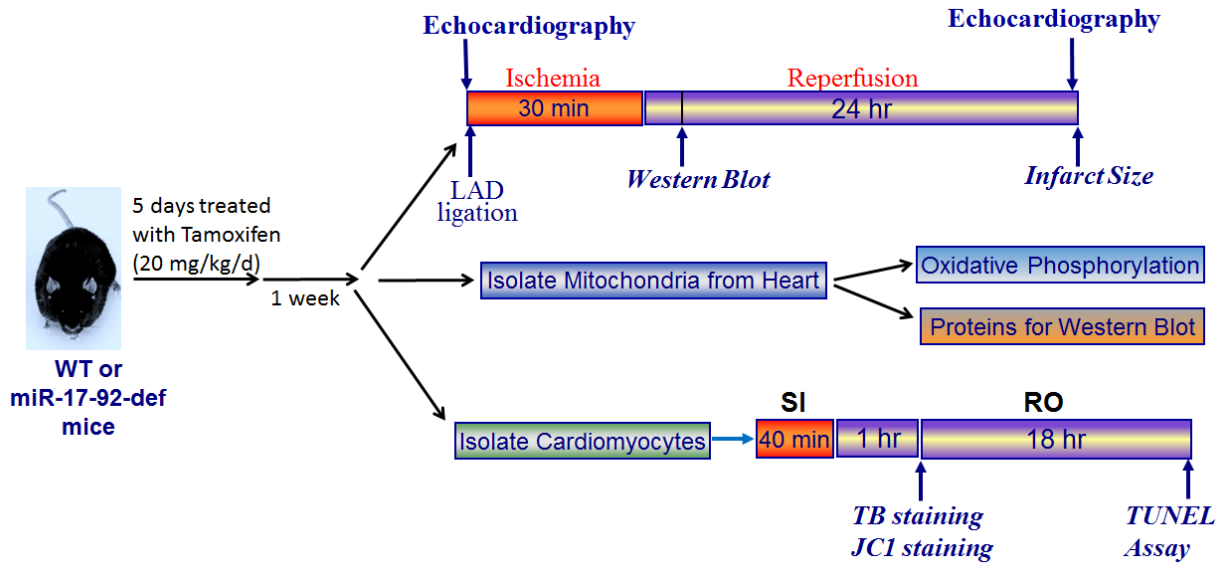


Figure 4: Experimental Design: *In vivo* studies included ischemia/reperfusion (I/R), measurements of cardiac function by echocardiography and quantitation of infarct size by triphenyl tetrazolium chloride (TTC) staining. *In vitro* experiments include mitochondrial oxidative phosphorylation studies and cardiomyocyte simulated ischemia and reoxygenation. Staining and protein analysis were achieved at different timepoints to measure apoptosis and protein targets.

2.4 Ischemia and Reperfusion via simulated Myocardial Infarction

The *in vivo* ischemia and reperfusion (I/R) protocols were accomplished by ligation of the left anterior descending coronary artery (LAD) and referenced by previously published methods⁵⁷. First, the mouse was anesthetized with pentobarbital sodium (70 mg/kg via intraperitoneal injection) and placed on a positive pressure ventilator. After ensuring the animal was unconscious, the left chest was opened at the fourth intercostal space and the pericardium was cut to visualize the heart. The LAD was then occluded for 30 minutes by placing a 2mm piece of polyethylene tubing (PE10) on top of the vessel and then tying a 7.0 silk ligature around the vessel and tubing. Reperfusion was accomplished by removing compression of the PE10 tube. The air was then expelled from the thoracic cavity and then the chest was closed using the silk ligatures. After a short period of time, the mouse was taken off the ventilator, and put into cage on a heating pad until regaining consciousness. Then the mouse was left to reperfuse for 24 hours.

2.5 Infarct Size Measurement

After 24 hours of reperfusion following 30 minutes of ischemia, the heart was removed from an anesthetized mouse. The heart was then attached via the aorta onto a Lagendorff apparatus. First, a 37°C Krebs-Henseleit buffer was perfused through the coronary arteries to wash the excess blood from the heart. Thereafter, a 3 ml solution of triphenyl tetrazolium chloride (TTC) in isotonic phosphate buffer (pH 7.4) at 37°C was perfused into the heart. This solution will show the area at risk. TTC- positive areas are stained red, while the TTC- negative areas remain white indicating an infarct (necrosis). The ligature was then tightened to ligate the LAD again and ~1ml of 5% Phthalo blue dye was injected into the aorta until the non risk area of the heart appeared blue. Finally, the heart was infused with saline to wash out the excess dye. The heart was then placed into a -20°C freezer overnight. Immediately after removing the frozen hearts, a sharp blade cut the

heart from apex to base in approximately 1mm thick slices. The slices were fixed in a 10% neutral buffered formaldehyde with a weight placed on top. The slices sat for 4 to 24 hours before being photographed. The infarcted tissue, the risk area, and the remained tissue were analyzed and calculated by computer morphometry using ImageJ imaging software.

2.6 Echocardiography

To monitor cardiac function in each mouse, an echocardiogram was taken at baseline before surgery and 24 hours after ischemia. Mice were anesthetized with 2.5L/min Isoflurane. After placing the mouse on the conductive platform while continuing to administer 1.5L/min Isoflurane, hair was removed from the chest. Then using a 30-MHz probe, two-dimensional Doppler images were taken of the short parasternal axis view of the heart via M-mode and B-mode on the VisualSonics Vevo 2100 Imaging System. The echocardiograms were analyzed using Vevo LAB 1.7.1 by tracking ejection fraction (EF), fractional shortening (FS), left ventricular end diastolic diameter (LVEDD), and left ventricular end systolic diameter (LVESD).

2.7 RNA Isolation

Mice were treated with pentobarbital sodium (100 mg/kg intraperitoneally) until unconscious. The hearts were then extracted by cutting the thoracic cavity from the base. The hearts were then cleaned with phosphate-buffered saline (PBS), quickly put into a plastic bag, and placed into liquid nitrogen. Total RNA including small RNA was isolated from frozen mouse heart tissue of using miRNeasy mini kit according to manufacturer's protocol (QIAGEN Sciences, MD, USA catalog number 217804). Concentration and the purity of isolated RNA was checked using Nanodrop ND-1000 spectrophotometer (Agilent technologies, CA, USA). Briefly 10 ng of total RNA was subjected to a reverse transcription reaction with miRNA specific RT primer using a microRNA reverse transcription kit (Applied Biosystems, CA, USA). For mRNA quantification,

2 ug of total RNA was used for cDNA synthesis. Reverse transcription was performed either using stem loop specific micro-RT primer or hexamer under the following condition : 16°C for 30 minutes ; 42°C for 30 minutes and 85°C for 5 minutes. The obtained cDNA was subjected to real-time PCR using Taqman amplicon specific assay probe under the following PCR cycle condition: 95°C for 10 minutes; 95°C for 15 seconds and 60°C for 60 seconds. Real time PCR was performed using Roche Light cyclers 480 II (Roche Applied Science, IN, USA). Taqman miRNA/mRNA assay probe (Occ-miR-302a-UAAGUGCUUCCAUGUUUUGGUGA)[AD1] were used (Applied Biosystems, CA, USA) to determine the expression level of miRNA-17 and 20a and were normalized using sno-202.

Genomic Map

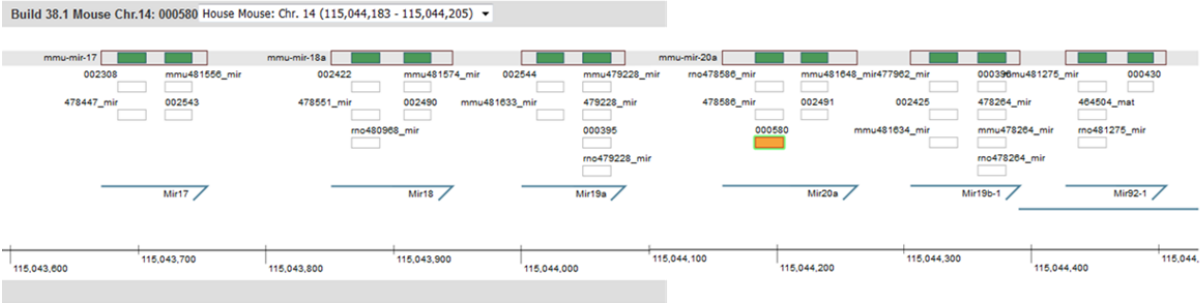


Figure 5⁵⁸: Genomic Map of Cluster miR-17-92 miR-20A (UAAAGUGCUUAUAGUGCAGGUAG; Assay ID- 000580) and miR-17 (CAAAGUGCUUACAGUGCAGGUAG; Assay ID- 002308) probes were developed based on the sequence upstream and downstream of these two miRNA. The housekeeping RNA used for comparison was snoRNA202 (GCTGTACTGACTTGATGAAAGTACTTTTGAACCTTTTCCATCTGATG; Assay ID- 001232).

2.8 Mitochondrial Isolation and Oxidative Phosphorylation Measurements

Isolated mitochondria were used to study the effects of miR-17-92 knockdown on oxidative phosphorylation⁵⁹. After removing the heart from an anesthetized mouse, it was rapidly placed in a cold buffer A (consisting of 100mM KCl, 50mM MOPS [3 (N morpholino) propanesulfonic acid], 1 mM EGTA, 5 mM MgSO₄, 1 mM ATP). The tissue was then homogenized in the buffer A by utilizing a Polytron tissue homogenizer for 3 seconds. A 1:1 solution of trypsin (5 mg/g tissue) and buffer B (buffer A + 0.2% bovine serum albumin) was then added to the homogenate before centrifugation at 500g for 10 minutes. The supernatant was again centrifuged at 3000g to precipitate mitochondria. The pellet was then washed with buffer B and KME (100 mM KCl, 50 mM MOPS, 0.5 mM EGTA). The activity of each complex was measured⁵⁹. The pellet was resuspended in KME for analysis, and glutamate+malate (complex I: 20 mM glutamate + 5 mM malate), succinate (complex II: 20 mM succinate with 7.5 μM rotenone) and complex IV substrate (1 mM N,N,N',N'-tetramethyl-p-phenylenediamine (TMPD)/20 mM L-ascorbate with 7.5 μM rotenone) as substrates to identify problems in the electron transport chain^{60,61}. Specifically, 2 mM azide was added to determine consumption of complex IV. State 3 (0.2 mM ADP-stimulated), state 4 (ADP-limited) respiration, respiratory control ratio (RCR), maximal rate of state 3 respiration (2 mM ADP and for TMPD/ascorbate), and rate of uncoupled respiration (0.04 mM dinitrophenol, DNP) were measured^{60,61}. The ratio of stimulated state3 and state4 respiration determined the Respiratory Control Ratio (RCR)^{60,61}.

Oxygen consumption of mitochondria was measured using a previously reported methodology⁶¹. A Clark-type oxygen electrode (Strathkelvin Instruments, North Lanarkshire, UK) was placed in a respiration buffer at 30 °C (80 mM KCl, 50 mM MOPS, 1 mM EGTA, 5 mM KH₂PO₄, 1 mg/ml defatted BSA) at pH 7.4 to measure the intact mitochondria oxygen needs⁶⁰.

2.9 Cardiomyocyte Isolation

Cardiomyocytes were isolated from mice (about six months to a year old) based on a protocol modified from previously published techniques^{62,63}. The mice were anesthetized with pentobarbital sodium (100 mg/kg intraperitoneally), and only the heart was excised from the thoracic cavity. Within a few minutes, the aorta was washed with bicarbonate buffer to clear excess blood and cannulated onto a Langendorff perfusion system⁶⁴. The hearts were perfused for approximately five minutes at a constant pressure of 55 mmHg with a Ca^{2+} -free bicarbonate-based buffer containing 120 mm NaCl, 5.4 mm KCl, 1.2 mm MgSO_4 , 1.2 mm NaH_2PO_4 , 5.6 mm glucose, 20 mm NaHCO_3 , 10 mm 2,3-butanedione monoxime, and 5 mm taurine that was continuously gassed with 95% O_2 + 5% CO_2 . Digestion of the heart was carried out for about 15 minutes by adding collagenase type II (Worthington; 0.5 mg/ml each) and protease type XIV (0.02 mg/ml) to the perfusion buffer. The heart was perfused for about another fifteen minutes after adding more $50 \mu\text{M}$ Ca^{2+} . Then, the heart was taken off the system, the ventricles were cut into smaller pieces, stirred, and gently aspirated with a transfer pipet to assist with cell dissociation. The solution was then centrifuged until a cell pellet was formed and resuspended in a three-step Ca^{2+} procedure with different concentrations of calcium (125, 250, and $500 \mu\text{M}$ Ca^{2+}). A sterilized minimum essential medium (catalogue number M1018, pH 7.35–7.45; Sigma) consisting of 1.2 mM Ca^{2+} , 12 mm NaHCO_3 , 2.5% fetal bovine serum, and 1% penicillin-streptomycin was then added to these isolated cardiomyocytes before being plated into 35-mm cell culture dishes. These dishes had been coated with $20 \mu\text{g/ml}$ mouse laminin in phosphate-buffered saline on a rocker for 1 hour. Prior to beginning the experiment, the cardiomyocytes were incubated for 1 hour in a humidified 5% CO_2 chamber to attach to the plate surface.

2.10 Cardiomyocyte Simulated Ischemia and Reoxygenation

The quality of isolated cardiomyocytes in the cell culture dishes was first quickly confirmed under a microscope. The cardiomyocytes were then subjected to simulated ischemia for 40 min by first replacing the cell medium with an “ischemia buffer”. This buffer was made by mixing 137.88 mg NaCl, 40 mg NaHCO₃, 2.4 mg NaH₂PO₄, 50 µl CaCl₂-2H₂O, 4.8 mg MgCl₂, 34 µl sodium lactate, 23.856 mg KCl, 32.84 mg 2-deoxyglucose and 20 ml of ultrapure water (pH adjusted to 6.2 and sterilized). Then the cells underwent 40 minutes of simulated ischemia in a 37 °C incubator by adjusting the gas to 1-2% O₂ and 5% CO₂. Reoxygenation was accomplished by replacing the ischemic buffer with normal medium in normoxic conditions. Assays for assessment of cell necrosis and MPTP were then stained after 1 hour and the apoptosis assay stain was applied after 18 hours of additional incubation.

2.11 TB staining

Trypan blue (TB) staining was used to observe cell viability by comparing the cells that were permeable to the dye to the healthy cells that excluded it. After 1 hour of reoxygenation, 15 µl of TB dye was added into the wells and incubated for 15 minutes (purchased from Sigma™ catalog number T8154). The myocytes were visualized under a Nikon Eclipse Ti-s microscope with a white light.

2.12 TUNEL staining

To analyze cardiomyocyte apoptosis, a nuclear DNA fragmentation detection kit via a fluorescence assay was utilized (purchased from Clontech™ catalog number 630108). The nuclear breaks were made by terminal transferase-mediated dUTP-digoxigenin nick end labeling (TUNEL) and TdT incorporates fluorescein- dUTP at the free 3'-hydroxyl ends of fragmented DNA. After 18 hours of reoxygenation, the cells in the chamber slides were fixed with 4%

formaldehyde/phosphate-buffered saline and placed in 4° for 25 minutes. Then, according to the manufacturer's protocol, cells were permeabilized by treating in prechilled 0.2% TritonX-100/PBS for 5 min on ice. Then, the slides were washed with PBS in coplin jars for 5 minutes. The cells on the slide were then incubated with a combination of equilibration buffer, nucleotide mix (containing fluorescein-dUTP), and TdT enzyme for 1 hour at 37°C. The reaction was stopped by immersing slides in 2X SSC, the slide were then counterstained with Vectashield mounting medium with 4',6-diamidino-2-phenylindole (DAPI, a DNA intercalating dye for visualizing nuclei in fixed cells; catalogue number H1200, Vector Laboratories). The stained cells were viewed and analyzed under a Nikon Eclipse Ti-s microscope (wavelength 520 ± 20 nm).

2.13 JC-1 staining

To measure mitochondrial membrane potential, the cells were stained with a dye mixture, 5,5',6,6'-tetrachloro-1,1',3,3'-tetraethylbenzimidazolyl-carbocyanine iodide (JC-1), 125µl of dimethyl sulfoxide (DMSO), and 1x Assay buffer according to the manufacturer's protocol (kit purchased from BD™ Biosciences catalog number 551302). The cells were then incubated at 37 °C for 15 minutes. The stained cells were examined under a Nikon Eclipse Ti-s microscope with a blue Nikon intensilight C-HGFL fluorescent light. The depolarized mitochondrial membranes were indicated by a shift from red to green fluorescence as the JC-1 monomers utilized channels to enter the permeabilized membrane.

2.14 Protein Isolation and Western Blots

After mice were anesthetized, hearts were excised from the chest cavity and a Western Blot analysis was used that was previously recorded⁵⁷. Extraction buffer (1 ml of lysis buffer containing 20 mM Tris-HCl, pH 7.4, 150 mM NaCl, 1 mM Na₂EDTA, 1 mM EGTA, 1% Triton, 2.5 mM sodium pyrophosphate, 1 mM -glycerophosphate, 1 mM Na₃VO₄, 1 g/ml leupeptin, 0.2 mM

PMSF, and halt protease and phosphatase inhibitor mixture; Thermo Fisher Scientific Inc., Rockford, IL) was used to isolate total soluble protein from the whole heart tissue. A Bradford assay was utilized if needed to calculate the sample volume needed per well along with the Laemlli buffer (a ratio of 1:20 buffer to B-mercaptoethanol). Each sample was heated for 5 minutes in 98°C and centrifuged for 30 seconds. The samples were injected into the gel wells, with running buffer (A Tris/Glycine/SDS buffer diluted in a 1:20 ratio of deionized water) in the cartridges. Sodium dodecyl sulfate polyacrylamide gel electrophoresis (SDS-PAGE) over 1 hour at 180 volts denatured and separated 75µg protein from each sample. This was then transferred onto a nitrocellulose membrane (0.2µm pore size). A TBST buffer (one part TBS, one-twentieth part Tween 20, and nine parts deionized water), followed by Ponceau S were coated on top of the membrane, then washed with deionized water to visualize the protein lanes. The TBST buffer was added again and allowed to incubated for 5 minutes and rinsing, before repeating twice. 10 ml of blocking buffer (5% milk in 100 ml of TBST buffer) was added to the membrane and placed on a rocker for 1 hour. The blots were then rinsed in TBST buffer twice. The membrane was incubated overnight with primary antibodies (indicated in the following table 1) on a rocker. A 1:1000 dilution with 5% BSA was added onto the samples. The next day, the membrane was washed then incubated with horseradish peroxidase-conjugated secondary antibody (1:2,000 dilutions) for 1 h at room temperature. The blots were developed using a chemiluminescent system (ECL Plus; Amersham Bioscience). The blots were exposed using Kodak film, and Image J software computed the optical density of the protein bands.

Table 1: Primary and Secondary Antibodies for Western Blot Analysis Each primary antibody was purchased separately and used in conjunction with a secondary antibody to identify protein expression.

Primary Antibody	Full Name	Company	Development Animal	Secondary Antibody	Catalog Number
PTEN	Phosphatase and tensin homolog	Cell Signaling	Rabbit polyclonal	Anti-Rabbit in Donkey	9552
pAKT	Phospho-AKT (Ser473) or Protein Kinase B	Cell Signaling	Rabbit polyclonal	Anti-Rabbit in Donkey	9271
AKT	Total AKT or Protein Kinase B	Cell Signaling	Rabbit polyclonal	Anti-Rabbit in Donkey	9272
GAPDH	Glyceraldehyde 3-phosphate dehydrogenase	Santa Cruz	Rabbit polyclonal	Anti-Rabbit in Donkey	sc-25778
MDH	Malate Dehydrogenase	Cell Signaling	Rabbit polyclonal	Anti-Rabbit in Donkey	8610
GDH	Glutamate Dehydrogenase	Cell Signaling	Rabbit monoclonal	Anti-Rabbit in Donkey	12793
PDH	Pyruvate Dehydrogenase	Santa Cruz	Rabbit polyclonal	Anti-Rabbit in Donkey	sc-292543
Cox IV	Cytochrome c Oxidase	Cell Signaling	Rabbit polyclonal	Anti-Rabbit in Donkey	4844

2.15 Data Analysis and Statistics

Data was analyzed and presented using Prism statistical software. Statistical analysis to calculate significant values were performed using the one-way analysis of variance. Then pairwise comparisons of each group were taken using the Student-Newman-Keuls post hoc test. When the value given for p was less than 0.05, the comparison is deemed statistically significant.

Results

The purpose of these experiments was to examine the effects of cardiac miR-17-92 deficiency in ischemia/ reperfusion conditions. First, the mice with the necessary mutant strain and tamoxifen-inducible CRE recombinase needed to be separated.

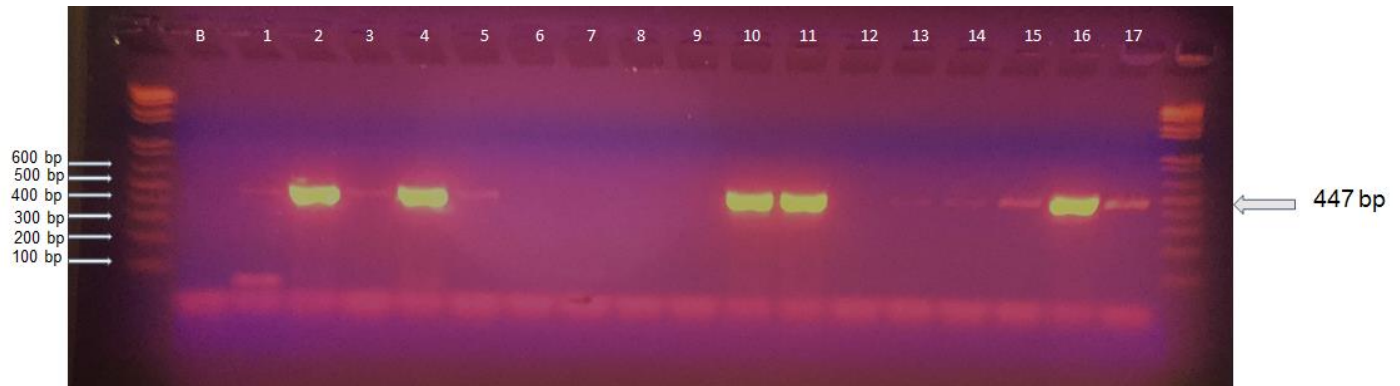


Figure 6: Representative figure of agarose gel with PCR products using CRE primers. Bright lines indicate presence of amplified DNA for comparison to end ladder lanes for appropriate sizing.

PCR- products (molecular weight: 447 bp) using following primers:
CRE (608-630): ATATCTCACGTACTGACGGTGGG,
CRE (1054-1032): CTGTTTCACTATCCAGGTTACGG

Genotyping of mice using CRE primers:

As shown in figure 6, the agarose gel (1.5 %) with PCR products using CRE primers indicated that mice tags with 2, 4, 10, 11 and 16 are positive for the tamoxifen-inducible CRE recombinase allele (447 bp band). Mice with tags number 1, 3, 5, 6, 7, 8, 8, 12, 13, 14, 15 and 17 are negative for CRE allele. The CRE primers check for the presence of the conditional knockout alpha-MHC-MerCreMer transgene on the alpha myosin heavy chain promoter. This promoter directs expression of CRE onto adult and juvenile cardiomyocytes during tamoxifen treatment. CRE will then act on loxP sites to delete a section of DNA. For mice that test positive for the cre recombinase allele, tamoxifen treatment will induce CRE. However, the confirmation of the loxP sites is also needed in order to ensure a conditional knockout.

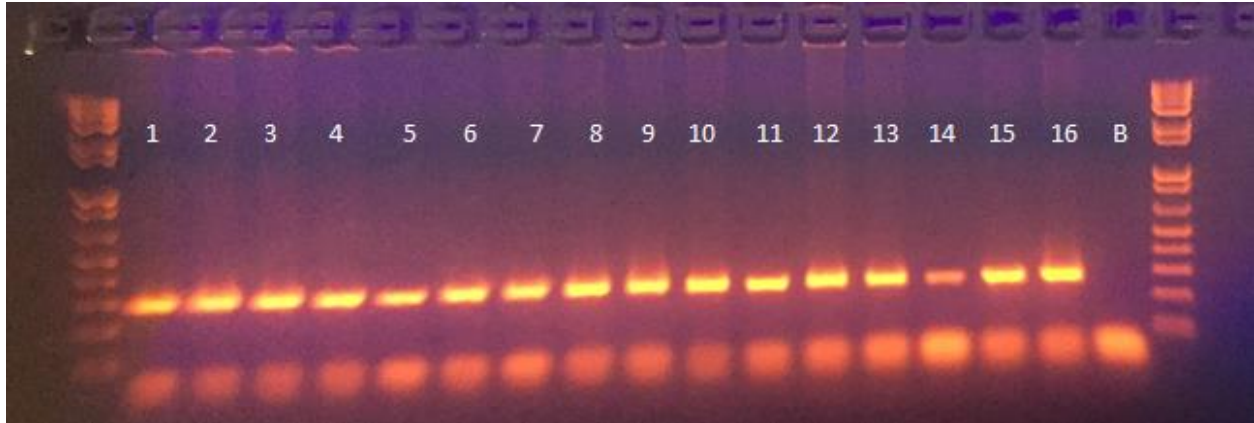


Figure 7: Representative Figure of Agarose Gel for Mutant miR-17-92 Cluster. Lanes 1-16 shows PCR products using the following three primers to identify the mice with flox/flox allele. Fl/Fl Mutant:289 bp, Heterozygote: 255 & 280 bp, WT: 255 bp. A conditional knockout that has been subjected to tamoxifen treatment will present at 441bp.

oIMR8528	TCG AGT ATC TGA CAA TGT GG	Common
oIMR8529	TAG CCA GAA GTT CCA AAT TGG	Wild type Reverse
oIMR8530	ATA GCC TGA AAC CAA CTG TGC	Mutant Reverse

Genotyping of mice for flox/flox allele:

As shown in figure 7, the agarose gel (1.7 %) indicated that mice tags with 1-16 were homozygous for the flox/flox allele (single band at 289 bp). Mice colonies with the flox/ flox allele were bred together to perpetuate the mutant transgene. These mice were also bred with both CRE positive and CRE negative alleles to promote genetic heterogeneity. The mutant transgene means that each miR-17-92 cluster is flanked by loxP sites, such that when CRE acts on the loxP sites it is deleted.

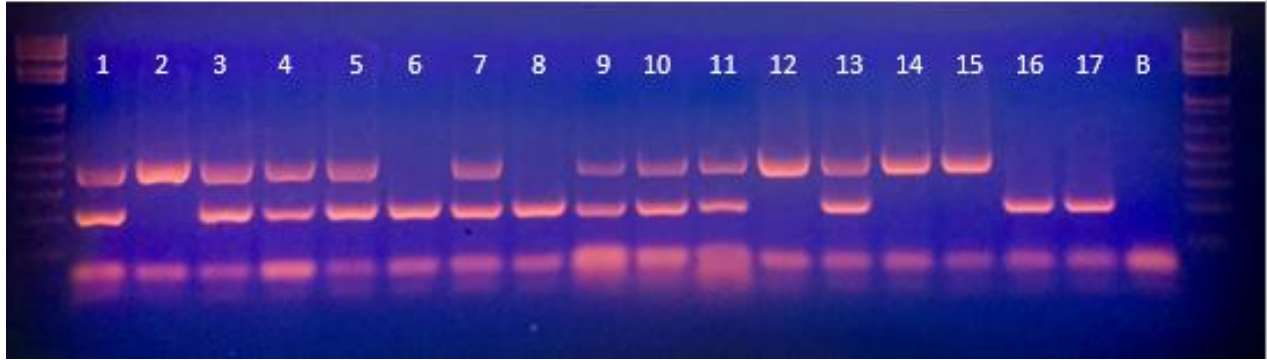


Figure 8: Representative Agarose Gel for Transgenic Genotyping. Lanes 1-17 contain PCR products using the following four primers to identify the mice with homozygous CRE (only 448 bp band), heterozygous CRE (both 448 bp and 230 bp bands) or non transgenic (only 230 bp band).

Genotyping with MYH6- CRE primers:

CRE (608-630): ATATCTCACGTA CTGACGGTGGG,

CRE (1055-1032): CCTGTTTCACTATCCAGGTTACGG,

A1CF (4879-4902): TTGGAGCTTCTGTTTCAGGCCATAG,

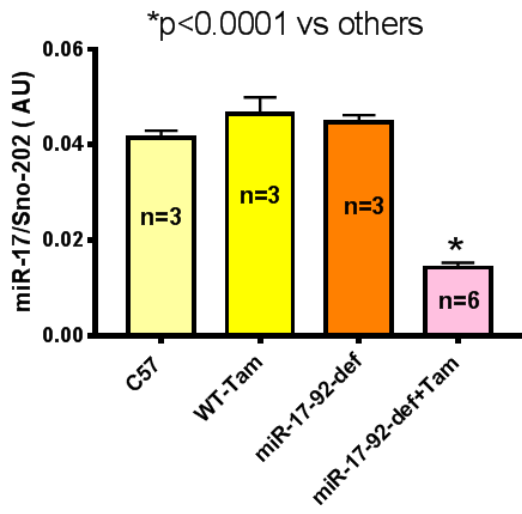
A1CF (5108-5085): TACCTGAGCAATTTCTGAGGTTCC,

CRE: 447 base pairs, Nontransgenic: 230 base pairs.

Genotyping of mice for homozygous CRE and heterozygous CRE:

As shown in Figure 8, the agarose gel (1.7 %) indicated used PCR products of DNA from mice hearts and 4 primers. Mice tags with 2, 12,14,15 are homozygous CRE positive, while mice tags 6, 8 16, and 17 are considered nontransgenic mice. The rest of the mice are heterozygous CRE positive mice, evidenced by two distinct bands. Homozygous CRE mice respond better to administration of tamoxifen. Due to low breeding numbers, both hemizygous and homozygous CRE mice were used in these experiments.

A.



B.

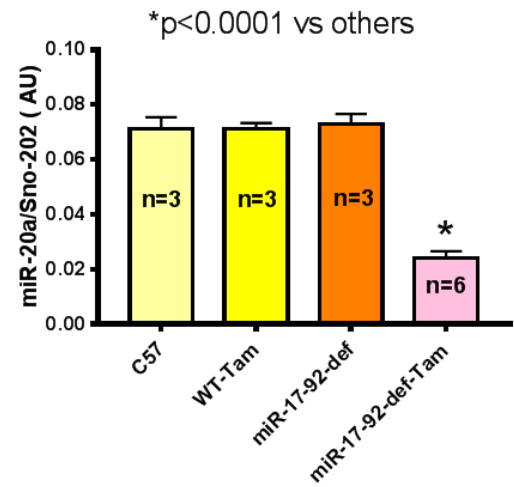


Figure 9: MicroRNAs in Hearts of WT and miR-17-92-def mice. Expression of (A) miR-17 and (B) miR-20a in C57, WT and miR-17-92-def following 1 week of completion of Tamoxifen treatment.

Expression of miR-17 and miR-20a following tamoxifen treatment:

After the tamoxifen treatment was given to the transgenic mice, miR-17-92 deficiency was checked using real-time PCR in comparison to a control group. Figure 9 shows the ratio of miR-17 to Sno-202 (A) and miR-20a to Sno-202 (B) in the hearts of C57, WT and miR-17-92-def mice following treatment with Tamoxifen (20 mg/kg/day for 5 days). The miR-17 and miR-20a expression were not altered between groups before tamoxifen treatment. However, both microRNAs were significantly reduced following tamoxifen treatment in miR-17-92-def mice. The WT mice that received tamoxifen treatment were used to compare the effect of the tamoxifen on the miR-17-92 cluster in mice that tested negatively for the CRE allele.

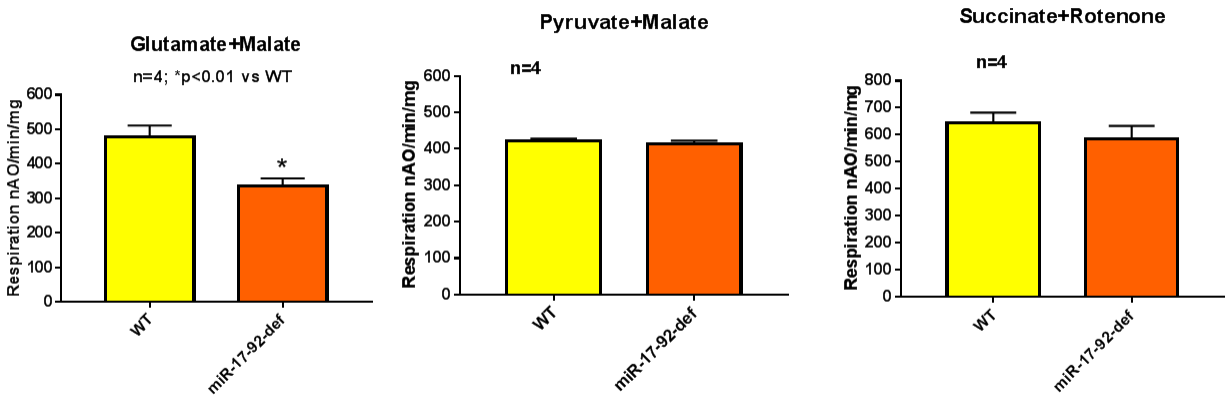


Figure 10: Mitochondrial Oxidative Phosphorylation. Function of complexes I (with substrates glutamate+malate) and II (pyruvate+malate) of the electron transport chain were observed following knockdown of the miR-17-92 cluster in mice.

Cardiac mitochondrial oxidative phosphorylation in WT and miR-17-20-def mice

To elucidate the effects of miR-17-92 knockdown on electron transport chain, mitochondrial oxidative phosphorylation were measured in isolated mitochondria of hearts of WT and miR-17-92-def mice after tamoxifen treatment. Figure 10 shows that compared to WT, oxidative phosphorylation was decreased using Glutamate+Malate as complex I substrate in the hearts of miR-17-92-deficient mice. However, there is no significant difference of oxidative phosphorylation using Pyruvate+Malate as well as succinate + rotenone suggesting that complex II remained unaffected in miR-17-92-deficient mice. In order to further understand oxidative phosphorylation dysregulation, each protein was studied further by determining concentrations via western blot.

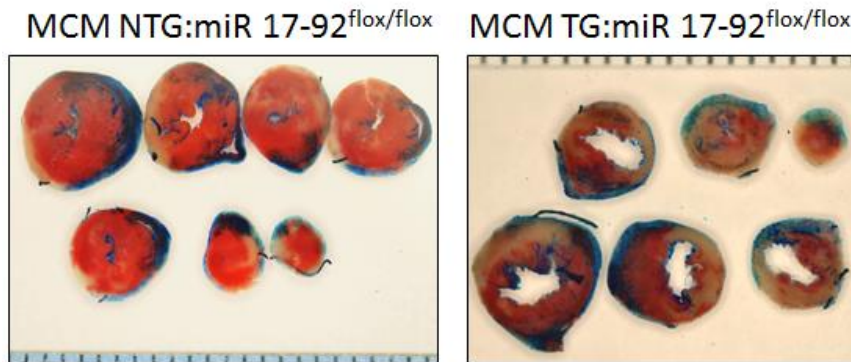
Table 2: Survival Rates of Mice. Below, WT and miR-17-92-def mice lives were tracked following 30 min ischemia (I) and reperfusion (R) surgery.

	Total	Survived following I/R	% of survival:
miR-17-92-def	31	15	48.38709677
WT	28	20	71.42857143

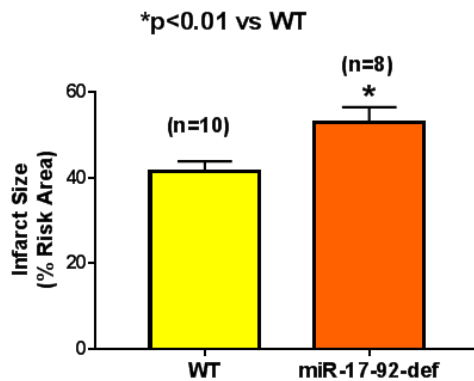
Myocardial injury following Ischemia/reperfusion injury in miR-17-92-deficient mice:

in vivo LAD ligation was performed to understand if the knock down of miR-17-92 had any effect on the survival of mice after 24 hours of reperfusion. A total of 59 mice were used in this study which included 31 miR-17-92-deficient and 28 WT mice. These mice were subjected to 30 minutes of LAD ligation and 24 hours of reperfusion (I/R). A total of 15 out of 31 miR-17-92-deficient mice survived following *in vivo* I/R by 30 minutes of LAD ligation and 24 hours reperfusion. Post I/R survival rate of miR-17-92 deficient mice is approximately 48 %. In contrast, the survival rate was significantly higher in WT mice where 20 out of 28 (or 71%) WT mice survived following *in vivo* I/R injury.

A



B



C

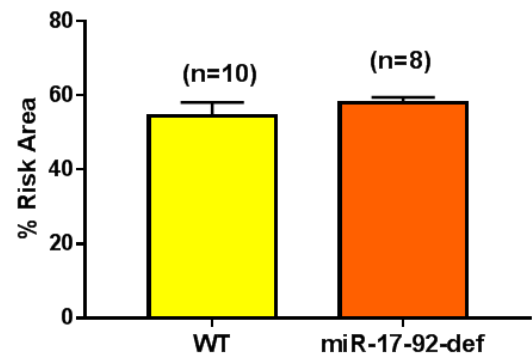


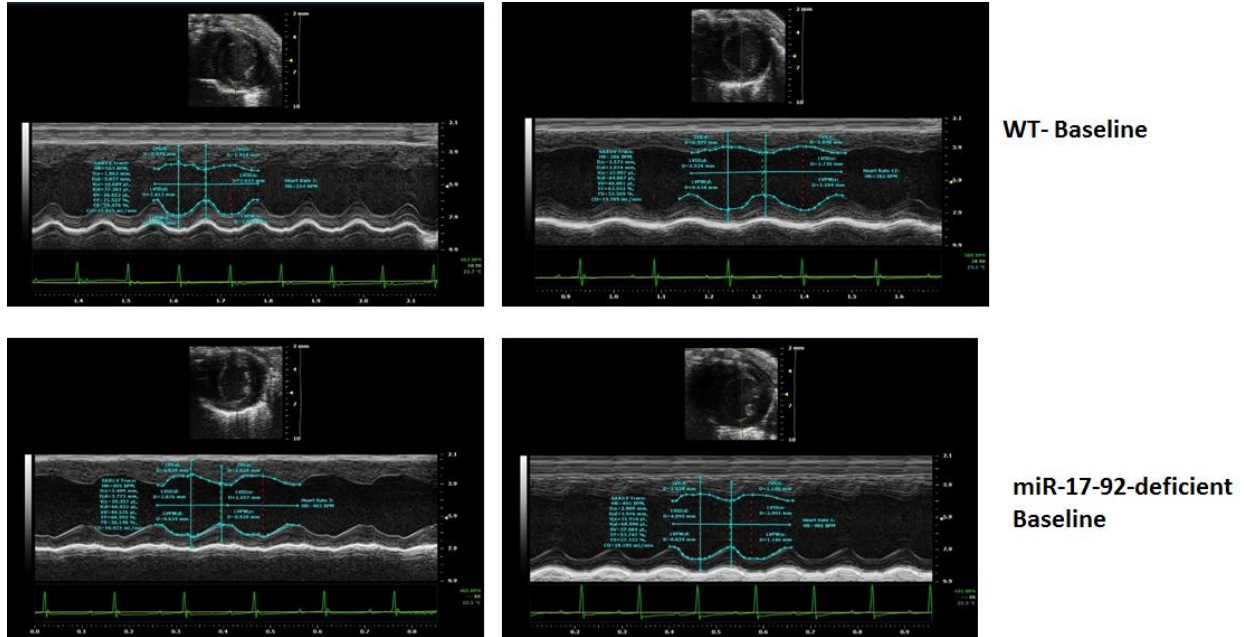
Figure 11: Infarct Size and Risk Area Measurement following I/R injury. A. Representative pictures of whole TTC and Phthalo blue staining of WT and miR-17-92-def mice hearts following 30 min of ischemia (I) and 24 hours of reperfusion (R). B. Infarct size as a percentage of risk area. C. Risk area as percent of the left ventricle.

Infarct Size and Cardiac Function after I/R injury:

The infarct size was also measured following 30 min of ischemia and 24 hours of reperfusion in WT and miR-17-92-def mice. As shown in Figure 11 A, Viable myocardium was stained bright red with TTC staining, while the white region was the infarcted myocardium. The blue region was demarcated as non-risk area. Infarct size was significantly increased in miR-17-92-deficient mice (52.9±3.6%) after I/R injury as compared to WT mice (41.6±2.2%) (Figure 11B). However, there

are no significant difference of the risk area between groups (Figure 11C). The red area indicated risk area that was exposed to ischemia via the LAD ligation. The purpose of measuring infarct size was to study how harmful the ischemia was to each heart and if the miR-17-92 changed responses in the event of a myocardial infarction.

A



B

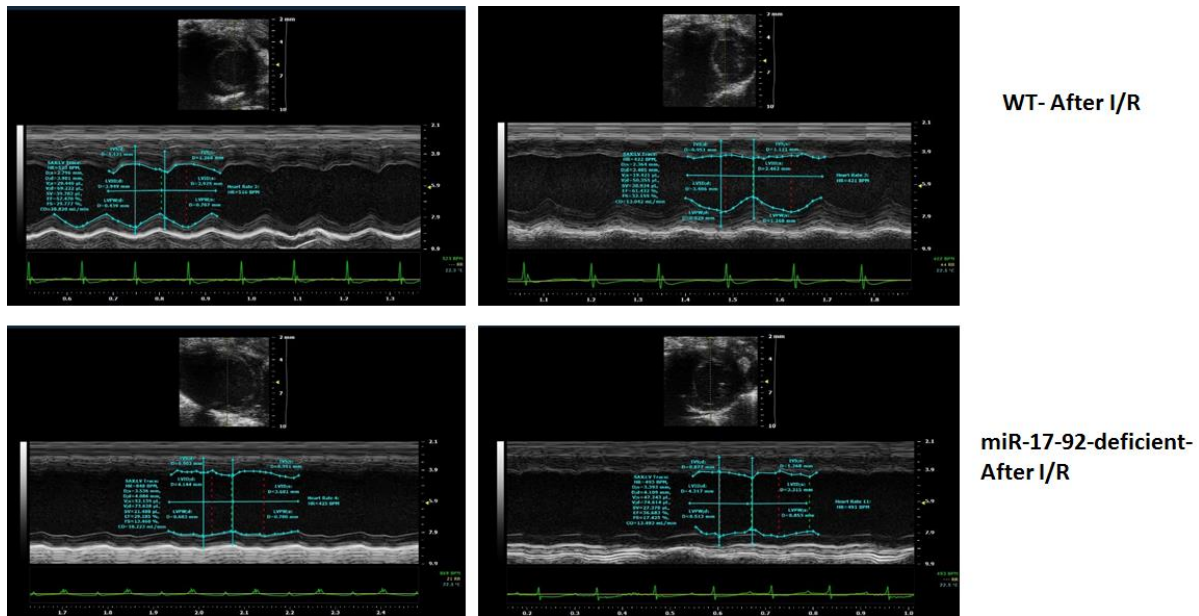
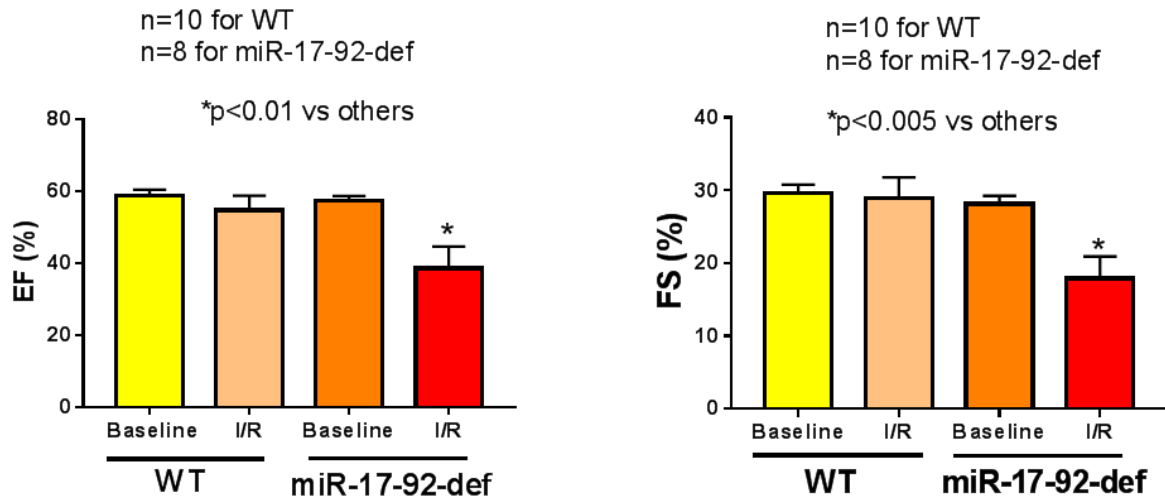


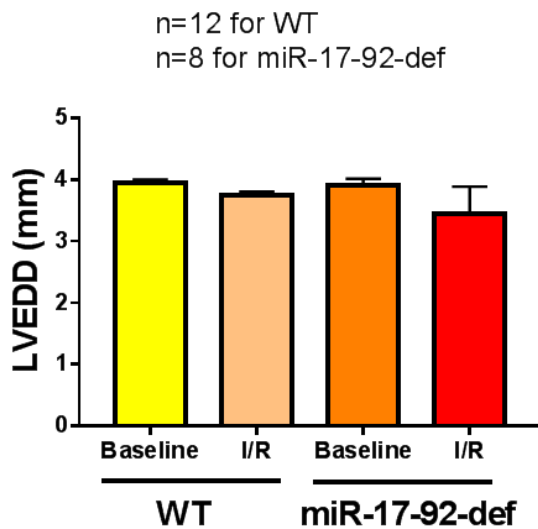
Figure 12: Cardiac Function of WT and miR-17-92-deficient Mice before I/R and after I/R Injury. A. Representative M-mode images demonstrating the LV contractility in WT and miR-17-92-def mice at baseline (Before I/R). B. Representative M-mode images demonstrating the LV contractility in WT and miR-17-92-def mice after 30 min ischemia and 24 hours of reperfusion.

A

B



C



D

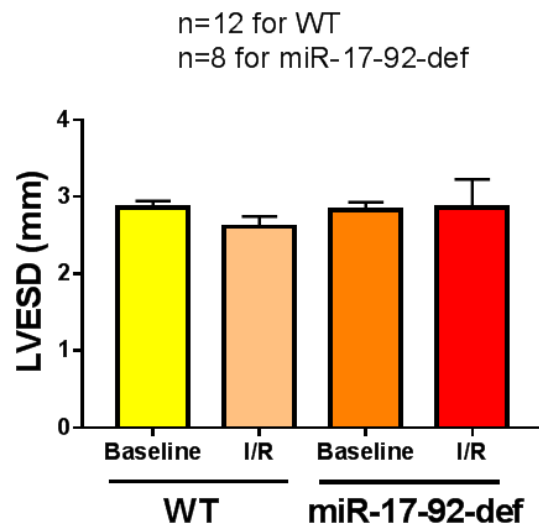


Figure 13: Cardiac Function of WT and miR-17-92 Mice before and after I/R. A. Percentage of Ejection Fraction (EF), B. Percentage of Fractional Shortening (FS), C. Left Ventricular End Diastolic Diameter (LVEDD) and D. Left Ventricular End Systolic Diameter (LVESD) were measured using at baseline and after I/R in both WT and miR-17-92-def mice.

Cardiac function was tested using echocardiograms and comparing measurements to a baseline.

This was studied to understand if there was heart failure occurring. Fractional Shortening (FS) was calculated as a percentage by subtracting LV end systolic diameter (LVESD) from LV end

diastolic diameter (LVEDD) and dividing by LVEDD. FS was significantly decreased in miR-17-92-def mice ($17.9 \pm 2.9\%$, $n=8$) after I/R as compared to all groups ($n=10$; $p < 0.005$) (Figure 13 B). Ejection Fraction (EF), a measurement of stroke volume and end diastolic volume, was found to be significantly decreased in miR-17-92-def mice ($38.6 \pm 5.9\%$) as compared to all others (WT-Baseline: $58.8 \pm 1.6\%$, WT- I/R: $54.62 \pm 2.9\%$ and miR-17-92-def-Baseline: $57.22 \pm 2.9\%$ 1.4% ; $p < 0.0.1$) as shown in Figure 13 A. The reduction of FS and EF indicated that miR-17-92 mice exhibited significant defect in cardiac function following I/R injury. Although, there were no significant differences of LVEDD and LVESD between groups (Figure 13 C, D).

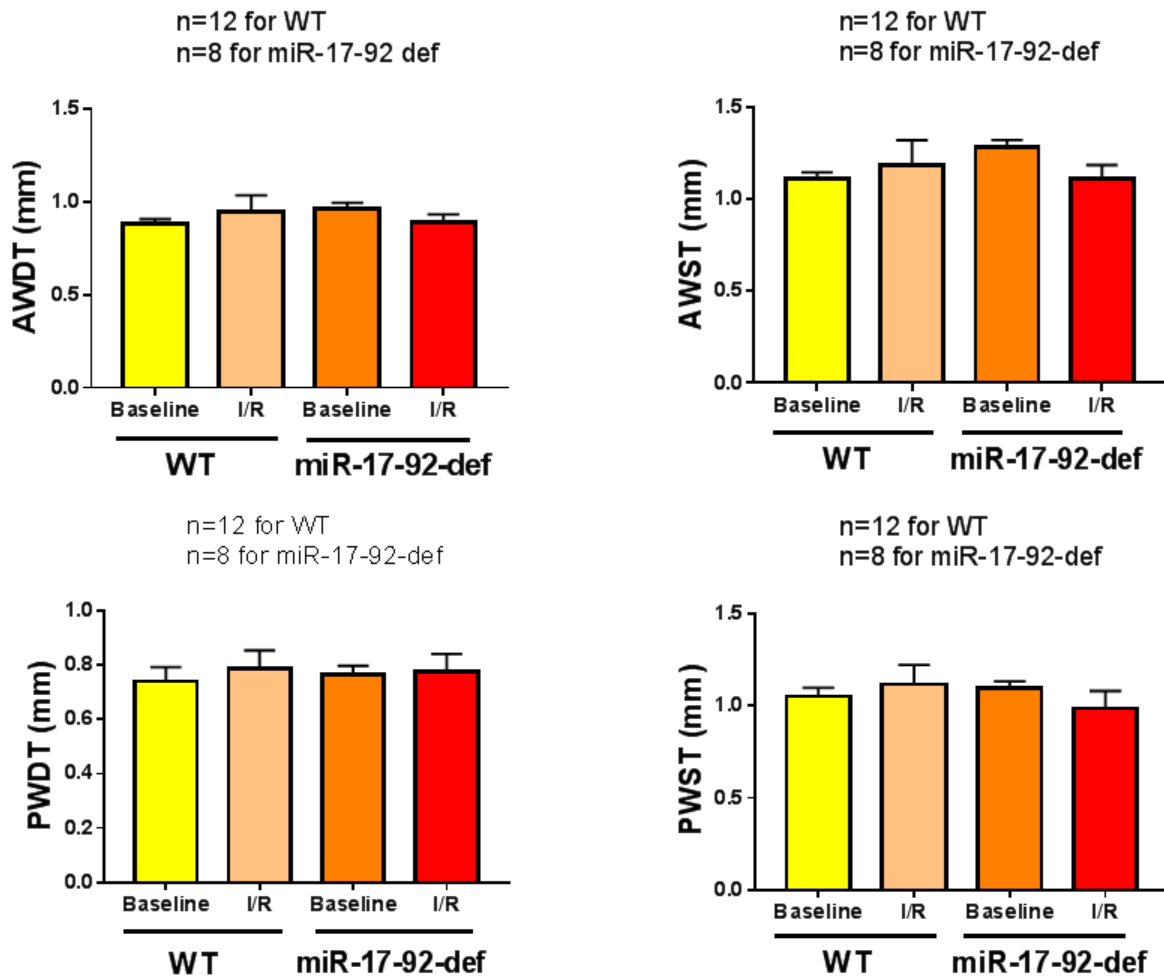
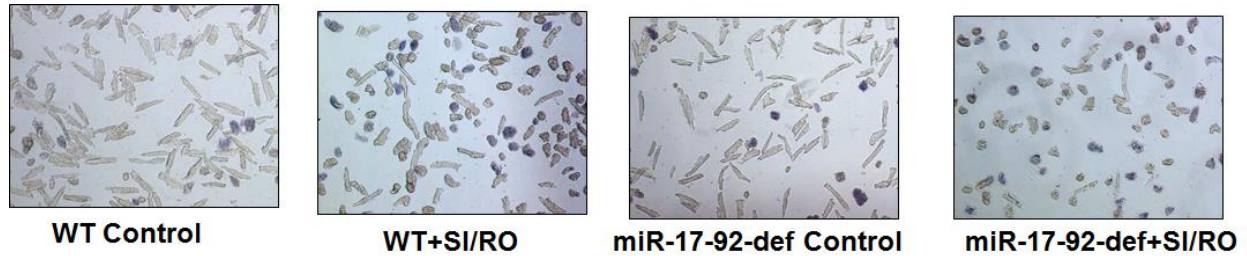


Figure 14: Echocardiography Measurement of Left Ventricle before and after I/R. Anterior wall diastolic thickness (AWDT), Anterior wall systolic thickness (AWST), Posterior wall diastolic thickness (PWDT) and Posterior wall systolic thickness (PWST) at baseline and post I/R in WT and miR-17-92-deficient mice.

Various other aspects of the left ventricle were measured before and after I/R to see if there were any significant changes to indicate either wall thinning or hypertrophy from adverse remodeling

in the heart due to ischemia. There were no significant differences of anterior wall diastolic thickness (AWDT), anterior wall systolic thickness (AWST), posterior wall diastolic thickness (PWDT) and posterior wall systolic thickness (PWST) at baseline and post I/R between WT and miR-17-92-deficient mice. The anterior wall was the top portion of the M-mode photograph taken in Figure 12, while the posterior wall was the bottom portion of the photograph. Diastole indicates that the heart is relaxed, the diastolic measurements were taken at the widest point. The systolic measurements were taken when the heart was most contracted, or the narrowest point.

A



B

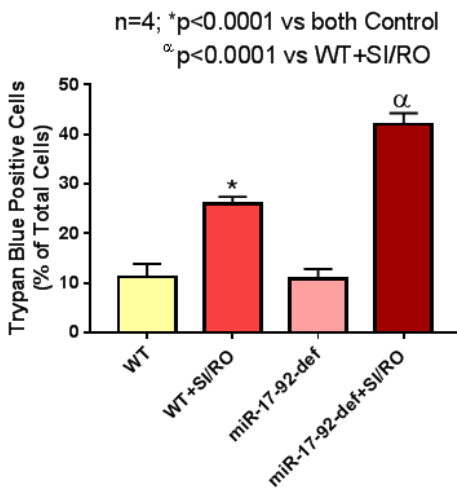


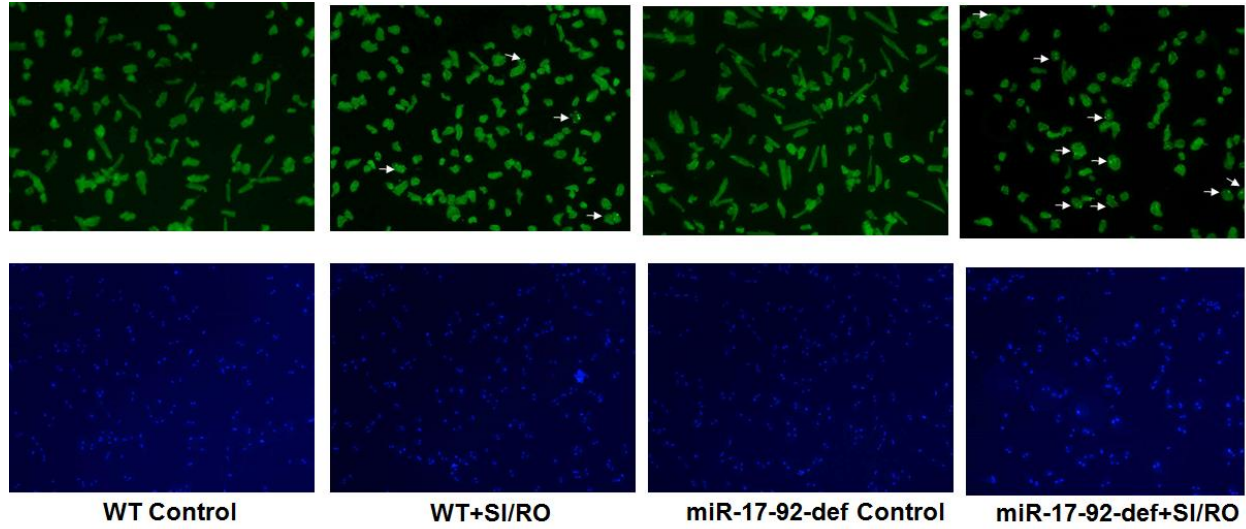
Figure 15: Assessment of Cardiomyocyte Necrosis by trypan blue (TB) Staining. A. Representative picture of TB staining of cardiomyocytes of WT and miR-17-92-def mice following 30 min simulated ischemia (SI) and 1 hour reoxygenation (RO). TB-positive cells (blue-positive myocytes) indicates necrotic cells. **B.** The percentage of trypan blue staining.

Effect of miR-17-92 deficiency on cardiomyocyte necrosis and apoptosis following simulated ischemia and reoxygenation:

The *in vitro* experiments were then performed to elucidate necrosis, apoptosis, and mitochondrial membrane potential after simulated ischemia and reperfusion in primary cardiomyocytes isolated from WT and miR-17-92-def mice following tamoxifen treatment. After 40 min SI and 1 hour RO, the percentage of trypan blue positive cardiomyocyte increased significantly isolated from both WT (25.8±1.5 %) and miR-17-92-def (42±2.3 %) mice as

compared to respective controls (WT: 11.2 ± 2.6 % and miR-17-92-def: 10.8 ± 2.1 %) (Figure 15). The necrosis was significantly higher in cardiomyocytes isolated from miR-17-92-def mice following SI/RO as compared to cardiomyocytes from WT mice ($n=4$, $p < 0.0001$). Necrosis is indicative of immediate cell death, and this test uses the broken plasma membrane to indicate necrotic cells.

A



B

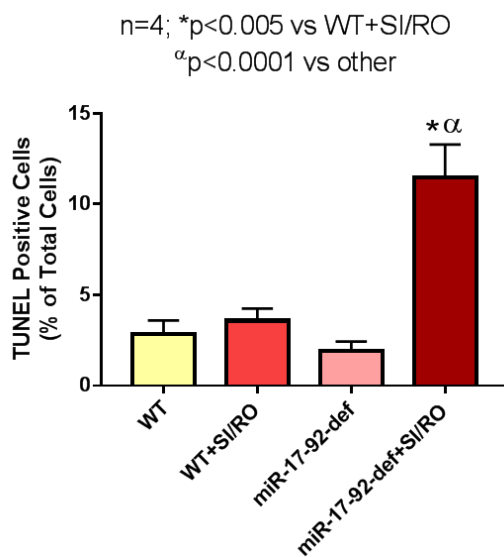
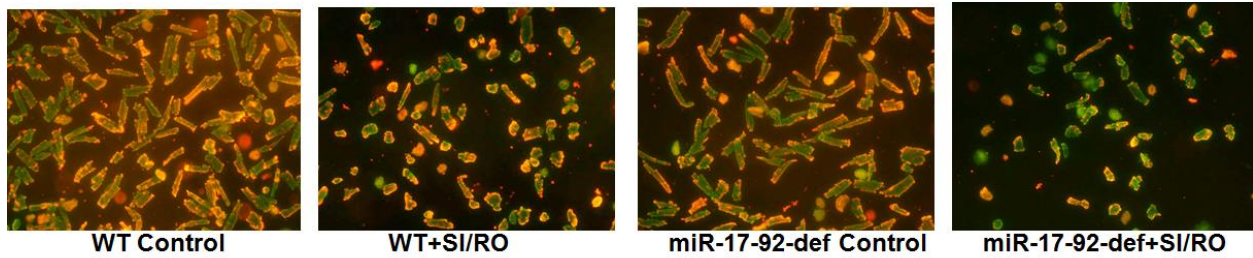


Figure 16: Assessment of Cardiomyocyte Apoptosis using TUNEL Staining. A. Representative pictures of adult cardiomyocytes of WT and miR-17-92-def mice following 30 min simulated ischemia (SI) and 18 hour reoxygenation (RO). Bright green fluorescent nuclei (FITC staining) indicates TUNEL positive cells (denoted by white arrows) and blue nuclei (DAPI staining) indicates total nuclei. B. The percentage of apoptosis.

Figure 16 shows that apoptosis, as indicated by TUNEL positive nuclei, was significantly higher in cardiomyocytes of both WT (3.5±0.6 %) and miR-17-92-def (11.5±1.8 %) mice

following SI/RO as compared to respective controls (WT: 2.8 ± 0.7 % and miR-17-92-def: 1.9 ± 0.5 %). Apoptosis was further exacerbated in cardiomyocytes of miR-17-92-def mice with SI/RO as compared to WT subjected to SI/RO, WT, and miR-17-92-def mice (n=4; $p < 0.0001$ vs others). These results suggest that cardiomyocytes isolated from the miR-17-92-def mice are more susceptible to SI/RO injury than cardiomyocytes of WT mice.

A



B

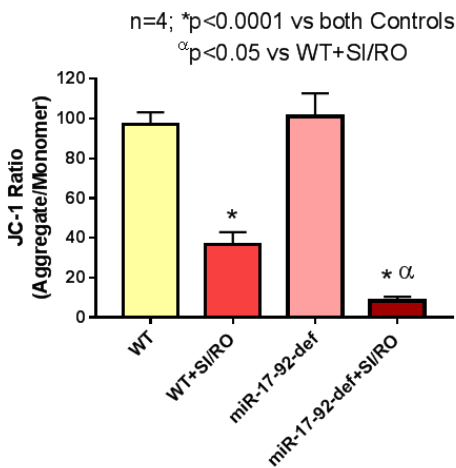


Figure 17: Assessment of Mitochondrial Membrane Potential using JC1 Staining. A. Representative picture of isolated cardiomyocytes from WT and miR-17-92-def mice were incubated with JC-1 staining following 40 min simulated ischemia (SI) and 1 hour reoxygenation (RO). The red cells are non-apoptotic cells with intact mitochondrial membrane potential. The green fluorescent cells are apoptotic or dead cells. **B.** Quantification of JC-1 aggregate/monomer ratio.

Effect of miR-17-92 deficiency on mitochondrial membrane potential in cardiomyocytes following SI/RO injury:

Cardiomyocyte apoptosis was also detected using a mitochondrial membrane potential ($\Delta\psi_m$) detection kit containing cationic lipophilic probe JC-1. The mitochondria of non-apoptotic cells appear in red following the aggregation of the JC-1 reagent, which emits red fluorescence at

590 nm (Figure 11). In contrast, in the apoptotic or dead cells, the JC-1 dye remains in its monomeric form, thereby emitting relatively more green fluorescence. As shown in Figure 17, there was a clear dissociation of JC-1 aggregates in the mitochondria of cardiomyocytes isolated from WT (36.5 ± 6.3 vs 97 ± 6.2) and miR-17-92-def (8.2 ± 2.2 vs 101.2 ± 11.6) mice following SI/RO injury as compared to their respective controls ($n=4$; $p < 0.0001$ vs controls). The ratio of JC-1 aggregates to monomer was significantly reduced in cardiomyocytes of miR-17-92-def mice as compared to cardiomyocytes of WT following SI/RO ($n=4$; $p < 0.05$ vs WT+SI/RO).

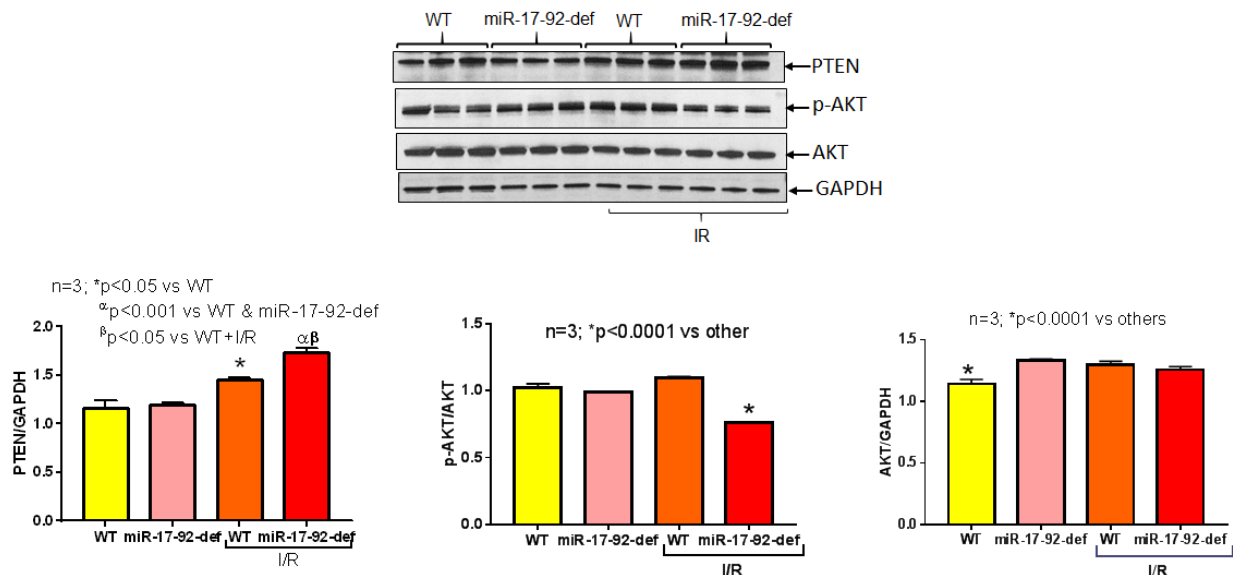


Figure 18: The Expression of miR-17-92 Downstream Targets PTEN and AKT. The first image is a representative immunoblots of WT and miR-17-92-def mice showing the expression of phosphatase and tensin homolog (PTEN), phosphorylated protein kinase B (p-AKT), total protein kinase B (AKT) and Glyceraldehyde 3-phosphate dehydrogenase (GAPDH). The lower panel showed the densitometric analysis of the ratios of PTEN/ GAPDH, pAKT/total AKT, and AKT/GAPDH.

Effect of miR-17-92 Deficiency on its Downstream Targets PTEN and AKT

Hearts after ischemia and reperfusion were used to identify the expression of proteins that were possible targets of miR-17-92. Figure 18 shows a significant increase in expression of PTEN following I/R in WT mice as compared to controls. Additionally, the induction of the expression of PTEN in miR-17-92-def mice was more prominent as compared to WT mice following I/R injury. Moreover, miR-17-92-def mice had significantly decreased expression of p-AKT as compared to WT mice following I/R injury and WT/ miR-17-92-def mice before I/R injury. Finally, total AKT was significantly lower in WT mice before I/R as compared to all other groups.

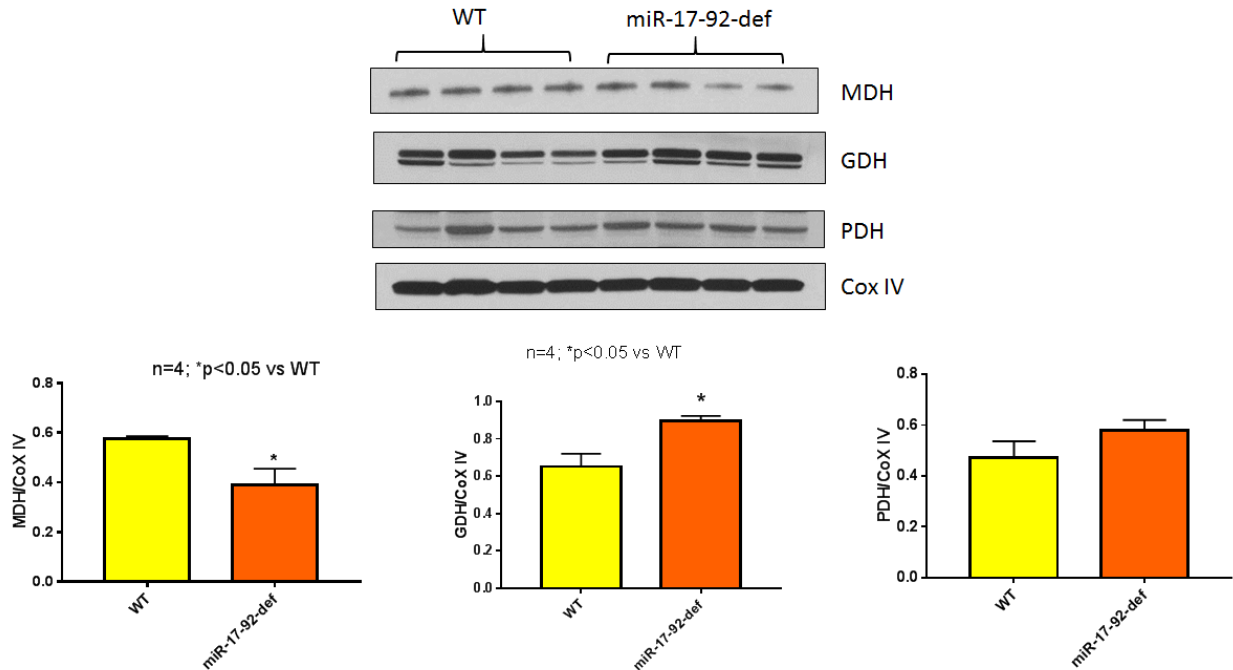


Figure 19: The Expression of MDH, GDH and PDH in Cardiac Mitochondria of WT and miR-17-92-def Mice. Representative immunoblots showing the expression of Malate Dehydrogenase (MDH), Glutamate Dehydrogenase (GDH), Pyruvate Dehydrogenase (PDH) and Cox IV. The lower panel showed the densitometric analysis of the ratios of MDH/Cox IV, GDH/Cox IV and PDH/Cox IV.

The expression of MDH, GDH and PDH in cardiac mitochondria of WT and miR-17-92-def mice

Figure 19 indicated there was a significant reduction of malate dehydrogenase expression in mitochondria of miR-17-92-def mice hearts as compared to WT. Additionally, there is a significant induction of glutamate dehydrogenase in mitochondria of miR-17-92-def mice hearts as compared to WT. There is no significant difference of pyruvate dehydrogenase between groups.

Discussion

CHD causes major strain to the healthcare system by leading to myocardial infarction and subsequent heart failure. The current therapy for treating myocardial infarctions is reperfusion, though this treatment itself can lead to negative consequences such as apoptosis and necrosis. The rapid return to physiological pH during reperfusion causes the engagement of pro-apoptotic factors that end in programmed cell death. Mitochondrial dysregulation due to the generation of reactive oxygen species and membrane depolarization release indicators for a caspase cascade. This delayed cell death can cause the left ventricle to become weaker as myocytes do not regenerate, leading to remodeling and heart failure.

MicroRNA have emerged as novel regulators of the process of cardiac growth and function. Through binding to mRNA sequences, their role often includes post-transcriptional gene expression by binding to the 3'UTR and precipitating degradation or inhibition. MiR-17-92 has emerged as an instrumental regulator of cardiac development and cancer through bypassing apoptosis through several factors such as Bax, Bcl-2, Bim, and PHD3. PTEN was also identified as a potential target and is important in regulating cardiac contractility and the PI3K/AKT pathway. Some studies contradict these findings, and thus studying the deletion of the miR-17-92 cluster is imperative to finding innovative targeted therapies utilizing this gene, such as regulation of epigenetic networks⁶⁵. Because upregulation of miR-17-92 can improve cardiac function after a myocardial infarction, giving a miR-17-92 mimic could be an option to de-differentiate and proliferate cardiomyocytes⁶⁶. Overexpression of this family was also proven to increase wall thickness, total cardiomyocyte number, and left ventricle dimension while during ischemia reperfusion was modestly cardioprotective²⁹. During cardiovascular morphogenesis, this constitutive overexpression can cause severe hypertrophic and a lethal cardiomyopathy³⁷. The

purpose was to investigate how the deletion of the miR-17-92 cluster determines myocardial infarction survival rates, infarct size, and apoptosis through proteins such as PTEN. The results of the miR-17-92 deletion in this study caused infarct size and apoptosis to increase as well as upregulation of PTEN. These significant results show that expression of pAKT and suppression of PTEN would be beneficial to a patient following myocardial infarction. Finding the right balance to overcome apoptosis, but not creating hypertrophy will be important in treating heart failure.

After ischemia and reperfusion via LAD ligation, survival rate was significantly reduced in miR-17-92 deficient mice (48%) compared to WT mice (71%). The miR-17-92 cluster is important for survival not only in neonatal mice, but also in cases of simulated ischemia based on the results. Even among those mice that survived, cardiac functions such as Ejection Fraction and Fractional Shortening, were reduced with augmentation of myocardial infarct size in miR-17-92-def mice as compared to WT mice. These cardiac functions were measured using echocardiography before and after surgery, and indicate the beginning of heart failure as shown in figures 12 and 13. Thus, the miR-17-92 cluster can weaken the heart and further injury in the case of myocardial infarction.

After identifying and breeding CRE inducible miR-17-92 mice through genotyping, knockdown via tamoxifen was checked using real time PCR through heart samples. Significant differences in miR-17 and miR-20 levels were found between treated mice and all others groups, proving that the tamoxifen treatment was able to remove the miR-17-92 cluster from the heart. This meant that miR-17-92 would not be able to influence downstream targets. Several mitochondrial defects were identified as well as decreased survival rates, increased infarct size, and increased apoptosis and necrosis provided by *in vivo* and *in vitro* studies. Downstream targets

of PTEN and pAKT were upregulated and suppressed, respectively in mice after I/R, suggesting that miR-17-92 deletion increases apoptosis through inhibition of PI3K/AKT signaling. In miR-17-92-def mice, complex 1 showed dysregulation meaning that the instability of the electron transport chain could be a factor in increasing infarct size (even with similar risk areas) and apoptosis significantly after I/R or SIRO, respectively. Additionally, the mitochondria could play an even bigger role through its decrease in expression of malate dehydrogenase and increase in glutamate dehydrogenase. Overexpression of this cluster can perhaps be important to prevent apoptosis in patients dealing with myocardial infarction.

The TB staining shows that the higher concentrations of necrotic cells in miR-17-92-def myocytes were indicative of immediate cell death (due to the broken plasma membranes) contributing to a larger infarct size following ischemia and reperfusion (as shown in Figure 15). TUNEL staining for apoptosis showed higher amounts in miR-17-92-def following simulated ischemia and reperfusion significantly compared to both the control in these conditions and to the miR-17-92-def cardiomyocytes without simulated ischemia. This indicates that the cell death continues in the heart, leading to an even greater infarct size than necrosis alone. Both of these phenomena show that the larger infarct size from the miR-17-92-def mice is a result of the increased rates of apoptosis and necrosis. The further study of mitochondrial membrane changes shows that the increased apoptosis could be due to the loss of polarization. When this happens, contents from the mitochondria, like cytochrome c can be released and start a signaling pathway for apoptosis. The JC-1 staining showed that the mitochondrial membrane was not able to significantly aggregate the JC-1 reagent in comparison to miR-17-92-def group before simulated ischemia and both WT groups. This disruption of the membrane in ischemia and reperfusion is related to the diminished upstream regulators of PTEN.

The western blots of MDH, GDH and PDH in cardiac mitochondria showed that there was significantly decreased expression of MDH and significantly increased expression of GDH in miR-17-92-def mice. Both of the proteins that changed concentrations as shown in figure 19 are involved in the TCA cycle and help produce ATP. In the absence of oxygen, these proteins will not be able to fully execute their role and as they rely on electron acceptors such as NAD⁺ or NADP⁺. If these electron acceptors are not available, then these electrons could create free oxygen radicals and cause the mitochondria to dysfunction.

In cardiomyocytes, when AKT is phosphorylated it becomes activated and acts in the phosphorylation of Bad and regulation of cell cycle progression through p21^{3,50}. PTEN prevents the phosphorylation of AKT from PIP2 and PIP3, which prevents the rest of the signaling cascade from occurring thus leading increased apoptosis as the results of this study show³. In our present study, the western blots using PTEN and pAKT antibodies showed the increased concentration of PTEN both before and after IR in hearts of miR-17-92-def mice with the concomitant reduction of phosphorylation of AKT only after IR in hearts of miR-17-92-def mice. Ischemia and reperfusion (IR) cause the inhibition of pAKT signaling which leads to increased apoptosis and decreased contractility. These changes, as shown in Figure 18, demonstrate that the reverse signaling can happen in overexpression of miR-17-92 and may help with future therapies to reduce apoptosis and increase contractility following a myocardial infarction. Despite these results showing that the possibility of increased expression of miR-17-92 could change infarct size and contractility, recent evidence demonstrates that cardiac growth can occur in exercise due to overexpression of miR-17-3p, so inducing this cluster may not be protective in all cases⁶⁷. Perhaps using this cluster as a biomarker could be influential in diagnosing issues with heart failure. For example, miR-19b has been indicated as a potential biomarker for collagen cross-linking in heart failure patients⁶⁸. MiR-

19 has a myriad of roles such as cardiomyocyte proliferation and protection against ischemic injury^{68,69}.

Further studies need to be completed in order to fully construct the role of miR-17-92 in cardiac ischemia and reperfusion. For *in vivo* studies, more tissue samples from other areas of the mouse should be run through a real time PCR to ensure sole deletion of this cluster in the heart. A comparison for mitochondrial function after I/R surgery would be imperative to understand how the deletion of the miR-17-92 affects oxidative phosphorylation. Both WT and miR-17-92-def mice hearts after 24 hours of reperfusion should be analyzed. Additionally, an apoptotic assay via TUNEL staining would be necessary after I/R, especially at different timepoints to better resolve how the miR-17-92 cluster exacerbates infarct size. Finally, the *in vitro* studies should include a protein analysis from the myocytes after simulated ischemia and reoxygenation. This work could open up information on how to treat patients after a myocardial infarction or for those who are being treated with CHD. More work should be completed on side effects of these therapies, particularly in aging animal models would be imperative to ensure safety in humans. Target sensitivity would also need to be tested to understand appropriate concentrations of miRNA inhibitors and mimics⁷⁰.

References

1. National Center for Healthcare Statistics. *Health, United States, 2015, With Special Feature on Racial and Ethnic Health Disparities*. (Center for Disease Control, 2016).
2. WHO | The top 10 causes of death. (2017).
3. Crackower, M. A. *et al.* Regulation of myocardial contractility and cell size by distinct PI3K-PTEN signaling pathways. *Cell* **110**, 737–749 (2002).
4. Hausenloy, D. J. & Yellon, D. M. Myocardial ischemia-reperfusion injury: a neglected therapeutic target. *J. Clin. Invest.* **123**, 92–100 (2013).
5. Li, S.-H. *et al.* miR-17 targets tissue inhibitor of metalloproteinase 1 and 2 to modulate cardiac matrix remodeling. *FASEB J.* **27**, 4254–4265 (2013).
6. Piper, H. A fresh look at reperfusion injury. *Cardiovasc. Res.* **38**, 291–300 (1998).
7. Salvesen, G. S. & Dixit, V. M. Caspase activation: the induced-proximity model. *Proc. Natl. Acad. Sci. U. S. A.* **96**, 10964–10967 (1999).
8. Roth, W. & Reed, J. C. Apoptosis and cancer: when BAX is TRAILing away. *Nat. Med.* **8**, 216–218 (2002).
9. Kim, J.-S., He, L. & Lemasters, J. J. Mitochondrial permeability transition: a common pathway to necrosis and apoptosis. *Biochem. Biophys. Res. Commun.* **304**, 463–470 (2003).
10. McCully, J. D., Wakiyama, H., Hsieh, Y.-J., Jones, M. & Levitsky, S. Differential contribution of necrosis and apoptosis in myocardial ischemia-reperfusion injury. *Am. J. Physiol. Heart Circ. Physiol.* **286**, H1923–35 (2004).
11. Alberts, B. *et al.* *Molecular Biology of the Cell, Sixth Edition*. (Garland Science, 2014).
12. Lesnefsky, E. J., Chen, Q., Tandler, B. & Hoppel, C. L. Mitochondrial Dysfunction and Myocardial Ischemia-Reperfusion: Implications for Novel Therapies. *Annu. Rev.*

- Pharmacol. Toxicol.* **57**, 535–565 (2017).
13. Widimsky, P. *et al.* Reperfusion therapy for ST elevation acute myocardial infarction in Europe: description of the current situation in 30 countries. *Eur. Heart J.* **31**, 943–957 (2010).
 14. Sun, L., Fan, H., Yang, L., Shi, L. & Liu, Y. Tyrosol prevents ischemia/reperfusion-induced cardiac injury in H9c2 cells: involvement of ROS, Hsp70, JNK and ERK, and apoptosis. *Molecules* **20**, 3758–3775 (2015).
 15. Yu, P. *et al.* Protective Effect of Sevoflurane Postconditioning against Cardiac Ischemia/Reperfusion Injury via Ameliorating Mitochondrial Impairment, Oxidative Stress and Rescuing Autophagic Clearance. *PLoS One* **10**, e0134666 (2015).
 16. Becker, L. B., vanden Hoek, T. L., Shao, Z. H., Li, C. Q. & Schumacker, P. T. Generation of superoxide in cardiomyocytes during ischemia before reperfusion. *Am. J. Physiol.* **277**, H2240–6 (1999).
 17. Sawyer, D. B. *et al.* Role of oxidative stress in myocardial hypertrophy and failure. *J. Mol. Cell. Cardiol.* **34**, 379–388 (2002).
 18. Boggs, R. M., Moody, J. A., Long, C. R., Tsai, K. L. & Murphy, K. E. Identification, amplification and characterization of miR-17-92 from canine tissue. *Gene* **404**, 25–30 (2007).
 19. Lai, E. C. Micro RNAs are complementary to 3' UTR sequence motifs that mediate negative post-transcriptional regulation. *Nat. Genet.* **30**, 363–364 (2002).
 20. Zhao, Y. *et al.* Dysregulation of cardiogenesis, cardiac conduction, and cell cycle in mice lacking miRNA-1-2. *Cell* **129**, 303–317 (2007).
 21. Callis, T. E. *et al.* MicroRNA-208a is a regulator of cardiac hypertrophy and conduction in

- mice. *J. Clin. Invest.* **119**, 2772–2786 (2009).
22. Wang, J. *et al.* Cardiomyocyte overexpression of miR-27b induces cardiac hypertrophy and dysfunction in mice. *Cell Res.* **22**, 516–527 (2012).
 23. Liu, N. *et al.* microRNA-133a regulates cardiomyocyte proliferation and suppresses smooth muscle gene expression in the heart. *Genes Dev.* **22**, 3242–3254 (2008).
 24. Zhou, M., Cai, J., Tang, Y. & Zhao, Q. MiR-17-92 cluster is a novel regulatory gene of cardiac ischemic/reperfusion injury. *Med. Hypotheses* **81**, 108–110 (2013).
 25. Mendell, J. T. miRiad roles for the miR-17-92 cluster in development and disease. *Cell* **133**, 217–222 (2008).
 26. Wang, J. *et al.* Bmp signaling regulates myocardial differentiation from cardiac progenitors through a MicroRNA-mediated mechanism. *Dev. Cell* **19**, 903–912 (2010).
 27. Doebele, C. *et al.* Members of the microRNA-17-92 cluster exhibit a cell-intrinsic antiangiogenic function in endothelial cells. *Blood* **115**, 4944–4950 (2010).
 28. Inomata, M. *et al.* MicroRNA-17-92 down-regulates expression of distinct targets in different B-cell lymphoma subtypes. *Blood* **113**, 396–402 (2009).
 29. Chen, J. *et al.* mir-17-92 cluster is required for and sufficient to induce cardiomyocyte proliferation in postnatal and adult hearts. *Circ. Res.* **112**, 1557–1566 (2013).
 30. Chamorro-Jorganes, A. *et al.* VEGF-Induced Expression of miR-17-92 Cluster in Endothelial Cells Is Mediated by ERK/ELK1 Activation and Regulates Angiogenesis. *Circ. Res.* **118**, 38–47 (2016).
 31. O'Donnell, K. A., Wentzel, E. A., Zeller, K. I., Dang, C. V. & Mendell, J. T. c-Myc-regulated microRNAs modulate E2F1 expression. *Nature* **435**, 839–843 (2005).
 32. Sylvestre, Y. *et al.* An E2F/miR-20a autoregulatory feedback loop. *J. Biol. Chem.* **282**,

- 2135–2143 (2007).
33. Mu, P. *et al.* Genetic dissection of the miR-17 92 cluster of microRNAs in Myc-induced B-cell lymphomas. *Genes Dev.* **23**, 2806–2811 (2009).
 34. He, L. *et al.* A microRNA polycistron as a potential human oncogene. *Nature* **435**, 828–833 (2005).
 35. Dai, B. *et al.* STAT3 mediates resistance to MEK inhibitor through microRNA miR-17. *Cancer Res.* **71**, 3658–3668 (2011).
 36. Cho, W. C. S. *MicroRNAs in Cancer Translational Research.* (Springer Science & Business Media, 2011).
 37. Danielson, L. S. *et al.* Cardiovascular dysregulation of miR-17-92 causes a lethal hypertrophic cardiomyopathy and arrhythmogenesis. *FASEB J.* **27**, 1460–1467 (2013).
 38. Ventura, A. *et al.* Targeted Deletion Reveals Essential and Overlapping Functions of the miR-17~92 Family of miRNA Clusters. *Cell* **132**, 875–886 (2008).
 39. Frank, D. *et al.* MicroRNA-20a inhibits stress-induced cardiomyocyte apoptosis involving its novel target EglN3/PHD3. *J. Mol. Cell. Cardiol.* **52**, 711–717 (2012).
 40. Huang, G., Nishimoto, K., Zhou, Z., Hughes, D. & Kleinerman, E. S. miR-20a encoded by the miR-17-92 cluster increases the metastatic potential of osteosarcoma cells by regulating Fas expression. *Cancer Res.* **72**, 908–916 (2012).
 41. Liu, Y. *et al.* Prolyl hydroxylase 3 interacts with Bcl-2 to regulate doxorubicin-induced apoptosis in H9c2 cells. *Biochem. Biophys. Res. Commun.* **401**, 231–237 (2010).
 42. Natarajan, R., Salloum, F. N., Fisher, B. J., Kukreja, R. C. & Fowler, A. A., 3rd. Hypoxia inducible factor-1 activation by prolyl 4-hydroxylase-2 gene silencing attenuates myocardial ischemia reperfusion injury. *Circ. Res.* **98**, 133–140 (2006).

43. Dews, M. *et al.* The Myc-miR-17 92 Axis Blunts TGF Signaling and Production of Multiple TGF -Dependent Antiangiogenic Factors. *Cancer Res.* **70**, 8233–8246 (2010).
44. Razumilava, N. *et al.* miR-25 targets TNF-related apoptosis inducing ligand (TRAIL) death receptor-4 and promotes apoptosis resistance in cholangiocarcinoma. *Hepatology* **55**, 465–475 (2012).
45. Bonauer, A. *et al.* MicroRNA-92a controls angiogenesis and functional recovery of ischemic tissues in mice. *Science* **324**, 1710–1713 (2009).
46. Chen, C. Real-time quantification of microRNAs by stem-loop RT-PCR. *Nucleic Acids Res.* **33**, e179–e179 (2005).
47. Cantley, L. C. The Phosphoinositide 3-Kinase Pathway. *Science* **296**, 1655–1657 (2002).
48. Huang, J. & Kontos, C. D. PTEN modulates vascular endothelial growth factor-mediated signaling and angiogenic effects. *J. Biol. Chem.* **277**, 10760–10766 (2002).
49. Ma, J. *et al.* PTEN regulates angiogenesis through PI3K/Akt/VEGF signaling pathway in human pancreatic cancer cells. *Mol. Cell. Biochem.* **331**, 161–171 (2009).
50. Brittsan, A. G. & Kranias, E. G. Phospholamban and Cardiac Contractile Function. *J. Mol. Cell. Cardiol.* **32**, 2131–2139 (2000).
51. Cao, Z. *et al.* CpG-ODN, the TLR9 agonist, attenuates myocardial ischemia/reperfusion injury: involving activation of PI3K/Akt signaling. *Biochim. Biophys. Acta* **1832**, 96–104 (2013).
52. Ha, T. *et al.* TLR2 ligands induce cardioprotection against ischaemia/reperfusion injury through a PI3K/Akt-dependent mechanism. *Cardiovasc. Res.* **87**, 694–703 (2010).
53. Ha, T. *et al.* Lipopolysaccharide-induced myocardial protection against ischaemia/reperfusion injury is mediated through a PI3K/Akt-dependent mechanism.

- Cardiovasc. Res.* **78**, 546–553 (2008).
54. Lu, C. *et al.* Attenuation of cardiac dysfunction and remodeling of myocardial infarction by microRNA-130a are mediated by suppression of PTEN and activation of PI3K dependent signaling. *J. Mol. Cell. Cardiol.* **89**, 87–97 (2015).
 55. 005650 - STOCK A1cf/J. Available at: <https://www.jax.org/strain/005650>. (Accessed: 14th June 2017)
 56. 008458 - STOCK Mirc1/J. Available at: <https://www.jax.org/strain/008458>. (Accessed: 14th June 2017)
 57. Das, A. *et al.* Mammalian target of rapamycin (mTOR) inhibition with rapamycin improves cardiac function in type 2 diabetic mice: potential role of attenuated oxidative stress and altered contractile protein expression. *J. Biol. Chem.* **289**, 4145–4160 (2014).
 58. Product Details. Available at: <http://www.thermofisher.com/order/genome-database/details/microrna/000580?CID=&ICID=>. (Accessed: 15th June 2017)
 59. Zhu, S.-G. *et al.* Dietary nitrate supplementation protects against Doxorubicin-induced cardiomyopathy by improving mitochondrial function. *J. Am. Coll. Cardiol.* **57**, 2181–2189 (2011).
 60. Lesnefsky, E. J. *et al.* Myocardial ischemia decreases oxidative phosphorylation through cytochrome oxidase in subsarcolemmal mitochondria. *Am. J. Physiol.* **273**, H1544–54 (1997).
 61. Chen, Q., Moghaddas, S., Hoppel, C. L. & Lesnefsky, E. J. Ischemic defects in the electron transport chain increase the production of reactive oxygen species from isolated rat heart mitochondria. *Am. J. Physiol. Cell Physiol.* **294**, C460–6 (2008).
 62. Dempsey, E. C. *et al.* Protein kinase C isozymes and the regulation of diverse cell

- responses. *Am. J. Physiol. Lung Cell. Mol. Physiol.* **279**, L429–38 (2000).
63. Xiao, R.-P. *et al.* Coupling of 2-Adrenoceptor to Gi Proteins and Its Physiological Relevance in Murine Cardiac Myocytes. *Circ. Res.* **84**, 43–52 (1999).
 64. Xi, L., Hess, M. L. & Kukreja, R. C. Ischemic preconditioning in isolated perfused mouse heart: reduction in infarct size without improvement of post-ischemic ventricular function. *Mol. Cell. Biochem.* **186**, 69–77 (1998).
 65. Xiao, J., Cretoiu, D., Lei, Z., Das, S. & Li, X. Genetic and Epigenetic Regulation Networks: Governing from Cardiovascular Development to Remodeling. *Biomed Res. Int.* **2017**, 1–2 (2017).
 66. Engel, F. B. *Heart Regeneration: Stem Cells and Beyond*. (World Scientific, 2012).
 67. Shi, J. *et al.* miR-17-3p Contributes to Exercise-Induced Cardiac Growth and Protects against Myocardial Ischemia-Reperfusion Injury. *Theranostics* **7**, 664–676 (2017).
 68. Beaumont, J. *et al.* MicroRNA-19b is a potential biomarker of increased myocardial collagen cross-linking in patients with aortic stenosis and heart failure. *Sci. Rep.* **7**, 40696 (2017).
 69. Gu, H., Liu, Z. & Zhou, L. Roles of miR-17-92 Cluster in Cardiovascular Development and Common Diseases. *Biomed Res. Int.* **2017**, 9102909 (2017).
 70. Jin, H. Y. *et al.* Differential Sensitivity of Target Genes to Translational Repression by miR-17~92. *PLoS Genet.* **13**, e1006623 (2017).

Vita

Meeta Bharati Prakash was born July 20, 1991 in Richmond, Virginia. She graduated from Phillips Exeter Academy in 2009. She received a double Bachelor of Arts in Biology and Environmental Studies from Dartmouth College in 2013. She worked at the Advisory Board Company as a healthcare consultant before joining Virginia Commonwealth University in 2015.